UCLouvain

École polytechnique de Louvain

Study of the effects of fluid injection around a NACA 23012 airfoil

Author : Hadrien Moreau
Supervisors : Philippe Chatelain, Jonas Vidaic, Grégoire Winckelmans
Reader : Vincent Legat
Academic year 2020-2021
Master [120] in Mechanical Engineering

Abstract

Flow separation is the main cause of loss of lift of aircraft's wings at high angles of attack. Active flow control is nowadays an important subject of study to try to replace the widely used high lift devices on aircraft. This thesis studied, using CFD tools, one kind of active flow control : the continuous blowing located close to the leading edge, used to delay the boundary layer separation on the suction side of a NACA23012 airfoil. A 2D baseline airfoil at a Reynolds number of 5.10^6 was built, simulated using ANSYS Fluent software (using k-ω SST turbulence model and assuming compressible flow), and the results were compared to experimental data. Multiple configurations of the continuous blowing with different momentum coefficients, velocity ratios, injection channel's widths, injection positions and injection angles were then built to assess their respective impact on the performances of the airfoil, compared to the baseline. An estimation of the power required to sustain the blowing was also provided.

The baseline proved to accurately predict the lift of the airfoil. The simulations showed that the continuous blowing is useful to delay the flow separation of up to 4°, from the initial critical angle of attack of 16°, improving the performances of the airfoil at high angles of attack. The analysis showed that the velocity ratio is an important parameter, as too low values are actually harmful to the performances. While the angle of injection does not seems to play a major part, a optimal injection angle of 15°with respect to the airfoil's surface was identified.

Keywords : Separation, Flow control, Continuous blowing, NACA23012, Lift

Contents

1 Introduction and context **6**

2 Generalities **7**
2.1 Introduction . . . 7
2.2 Reminder about airfoils and forces convention . . . 7
2.3 Physics of airfoil flow separation . . . 8
2.4 Air flow control strategies . . . 10
2.5 Literature review . . . 13

3 Methodology and modelization **14**
3.1 Introduction . . . 14
3.2 The CFD Tool . . . 14
3.3 Baseline model . . . 15
3.3.1 Geometry and mesh . . . 15
3.3.2 Problem definition and models choice . . . 18
3.4 Airfoil with blowing . . . 18
3.4.1 Geometry and mesh . . . 18
3.4.2 Problem definition and models choice . . . 20
3.4.3 Estimation of the power required for the blowing . . . 21

4 Results and discussion **23**
4.1 Introduction . . . 23
4.2 Baseline results and comparison with experimental data . . . 23
4.3 Airfoil with control results . . . 28
4.3.1 Impact of the momentum coefficient and velocity ratio of the blowing . . . 28
4.3.2 Impact of the injection slot's position . . . 35
4.3.3 Impact of the angle of injection . . . 38

5 Conclusion **42**

List of abbreviations and symbols

α	: Angle of attack of an airfoil, °
c	: Chord of an airfoil, m
$\overline{x}$	: $= \frac{x}{c}$ Dimensionless distance from the leading edge
V_∞	: Free stream velocity magnitude, m/s
$V_{\infty,x}$	: x component of the free stream velocity, m/s
$V_{\infty,y}$	: y component of the free stream velocity, m/s
ρ_∞	: Free stream density, kg/m^3
T_∞	: Free stream temperature, K
μ	: Dynamic viscosity, Pa.s
ν	: Kinematic viscosity, m^2/s
Re_∞	: Free stream Reynolds number
C_L	: Lift coefficient
C_D	: Drag coefficient
y^+	: Dimensionless wall distance
τ_w	: Wall shear stress, Pa
L_{inj}	: Injection channel width, m
β_{inj}	: Injection channel angle, with respect to the airfoil's skin, °
C_μ	: Momentum coefficient of the blowing
V_{inj}	: Design velocity of the blowing, m/s
VR	: Velocity ratio of the blowing
$P_{m,inj}$	: Power required to sustain the blowing, kW

List of Figures

1 Schematic of a wing : slat and flap . . . 6
2 Examples of many types of airfoils . . . 7
3 Description of an airfoil . . . 8
4 Illustration of the flow separation and recirculation phenomenon . . . 9
5 Illustration of a typical lift curve of an airfoil, with the stall point . . . 10
6 Example of passive air flow control actuator : Vortex generators on a Zodiac CH 601 HD wing . . . 11
7 Example of active flow control actuator : high lift devices on an airliner . . . 11
8 Schematic of the impact of the high lift devices on the lift coefficient of a wing . . . 12
9 AFC actuator : blowing in the boundary layer . . . 12
10 Geometry of the baseline's domain of computing . . . 16
11 Closer look at the mesh around the baseline NACA23012 airfoil's leading edge . . . 17
12 Closer look at the mesh around the baseline NACA23012 airfoil's trailing edge . . . 17
13 Schematic of the injection slot geometry, with the bevelled outlet . . . 19
14 Mesh close to the leading edge of the airfoil with blowing channel . . . 19
15 Closer look at the injection slot mesh . . . 20
16 Schematic of the model used to compute the power cost of the injection . . . 21
17 Convergence curve of the computation of the lift coefficient, baseline airfoil . . . 24
18 C_L versus α, baseline NACA23012 airfoil . . . 24
19 C_D versus α, baseline NACA23012 airfoil . . . 25
20 Baseline NACA23012 airfoil polar . . . 25
21 Lift to drag ratio versus α, baseline NACA23012 airfoil . . . 26
22 Velocity contour of the baseline NACA23012, $\alpha = 16°$ . . . 26
23 Velocity vectors above the trailing edge of the baseline NACA23012, $\alpha = 16°$ . . . 27
24 Wall shear stress distribution of the baseline NACA23012, $\alpha = 16°$ . . . 27
25 Comparison of the effect of the momentum coefficient and velocity ratio, lift vs α and drag vs α : $C_\mu = 0{,}5$ % . . . 30
26 Comparison of the effect of the momentum coefficient and velocity ratio, lift vs α and drag vs α : $C_\mu = 1{,}0$ % . . . 30
27 Comparison of the effect of the momentum coefficient and velocity ratio, lift vs α and drag vs α : $C_\mu = 1{,}5$ % . . . 31
28 Comparison of the effect of the momentum coefficient and velocity ratio, lift vs α and drag vs α : $C_\mu = 2{,}0$ % . . . 31
29 Power required for the control vs α : $C_\mu = 1{,}0$ % . . . 32
30 Power required for the control vs α : $C_\mu = 1{,}5$ % . . . 32
31 Relative gain of lift compared to the baseline vs required power : $C_\mu = 1{,}0$ % . . . 33
32 Relative gain of lift compared to the baseline vs required power : $C_\mu = 1{,}5$ % . . . 33
33 Velocity contour around the airfoil with AFC at $\overline{x}_{inj} = 3$ % : $L_{inj} = 1{,}5$ mm ; $C_\mu = 1{,}0$ % ; VR = 2,582 . . . 34
34 Velocity contour close to the injection slot at $\overline{x}_{inj} = 3$ % : $L_{inj} = 1{,}5$ mm ; $C_\mu = 1{,}0$ % ; VR = 2,582 . . . 34
35 Comparison of the effect of the injection position, lift vs α and drag vs α : $L_{inj} = 1{,}5$ [mm] ; $C_\mu = 1{,}0$ % . . . 35
36 Comparison of the effect of the injection position, lift vs α and drag vs α : $L_{inj} = 1{,}5$ [mm] ; $C_\mu = 1{,}5$ % . . . 36
37 Comparison of the effect of the injection position, lift vs α and drag vs α : $L_{inj} = 2{,}0$ [mm] ; $C_\mu = 1{,}5$ % . . . 36

38 Comparison of the effect of the injection position, lift vs α and drag vs α : L_{inj} = 2,0 [mm] ; C_μ = 2,0 % 37
39 Comparison of the effect of the injection angle : L_{inj} = 1,5 [mm] ; C_μ = 1,0 % ; $\overline{x}_{inj}$ = 2 % 38
40 Comparison of the effect of the injection angle : L_{inj} = 1,5 [mm] ; C_μ = 1,5 % ; $\overline{x}_{inj}$ = 2 % 39
41 Comparison of the effect of the injection angle : L_{inj} = 1,5 [mm] ; C_μ = 1,0 % ; $\overline{x}_{inj}$ = 3 % 39
42 Comparison of the effect of the injection angle : L_{inj} = 1,5 [mm] ; C_μ = 1,5 % ; $\overline{x}_{inj}$ = 3 % 40
43 Comparison of the effect of the injection angle : L_{inj} = 1,5 [mm] ; C_μ = 1,0 % ; $\overline{x}_{inj}$ = 4 % 40
44 Comparison of the effect of the injection angle : L_{inj} = 1,5 [mm] ; C_μ = 1,5 % ; $\overline{x}_{inj}$ = 4 % 41

List of Tables

1 Baseline mesh properties 16
2 Physical properties of the free stream 18
3 Injection channel mesh, and global mesh properties (airfoil with control) 19
4 Simulated configurations for the first part 28

1 Introduction and context

During the last decades, commercial airliners has taken an important part of transporting people and freight all around the world. In 2018, the aerial traffic reached 4,23 billions passengers and 220,7 billions tons-kilometres, which is more than ten times the traffic of 1970 [1]. Since the beginning of civil aircraft, airliners has been able to transport more passengers over larger distances, and has been equipped with more powerful motors, from the propellers to the turbo-fans. The fuel consumption of the airliners always has been a huge concern for the economical viability of aerial transport and the quite recent awareness about environment pollution and climate change has pushed up this concern to a vital point. For this reason, the companies invested billions of dollars to develop the performances of their airliners and to reduce their fuel consumption by improving the performances of existing components but also by developing innovative systems.

The wings of an aircraft are a major component which drive its aerodynamic performances, and thus play a huge part in the fuel consumption. For commercial airliners, they are usually optimized so that their drag is minimal when they are at their cruise speed and altitude while the lift is enough to maintain a level flight. The flaw of this optimization is that the lift produced by the wings at low speed conditions, like during the take-off and the landing, is not great enough to compensate the aircraft's weight. For this reason, the high lift devices (slats and flaps, see figure 1) has been developed to enhance the lift of the wings at take-off and landing, to the detriment of the drag. Their role is to enhance the lift and prevent the separation of the flow at higher angles of attack by modifying the geometry of the wings, in return of increased drag. These devices are only deployed during brief moments and are thus a dead weight of a few tons during the rest of the flight. They also represent a large cost for the aircraft (up to 11% of the aircraft total cost [2]) because of the building and maintenance. During the last two decades, new ways of improving the performances of the wings at low speed has been studied with the goal to replace these high lift devices with active air Flow Control (AFC), having the same effects on the aerodynamic performances at low speed and higher angles of attack, but a lower cost.

The SONACA (*Société Nationale de Construction Aerospatiale*) is a Belgian company which is part of the SONACA Group. The group has different business lines : the Defence for which they provide structure manufacturing and maintenance but also pilot training ; the Aerospace for which they are involved in satellite platform, payload and launcher; the Aeronautics for which they design, build and certify devices and systems for airliners, in particular the flaps and the slats but also spoilers, ailerons and anti-icing systems [3]. They are interested in developing their aerodynamics knowledge in air flow control and thus they suggested this subject as a master thesis. The present thesis aims at studying, using CFD tools, the effects of one type of active FC actuator : the continuous blowing, located close to the leading edge of a NACA23012 airfoil. Several parameters of the blowing will be investigated to understand their impact on the performances of the airfoil compared to a baseline without any control.

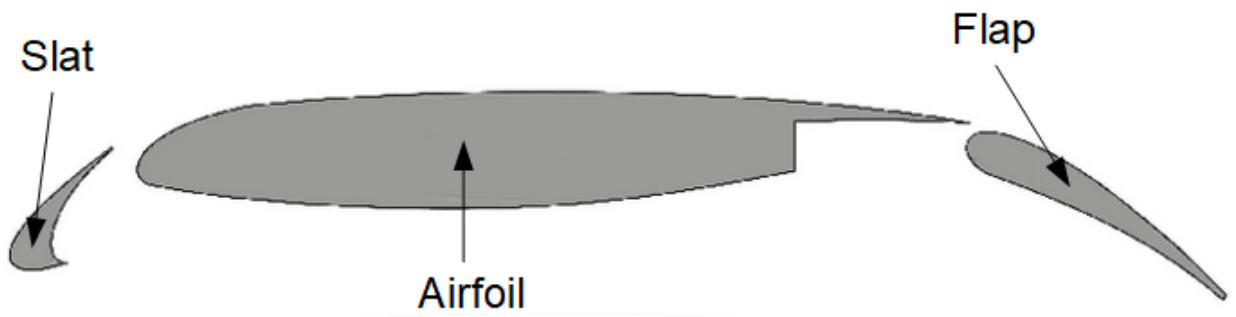

Figure 1: Schematic of a wing : slat and flap

2 Generalities

2.1 Introduction

In this chapter, I will recall basics about aerodynamics and airfoil, and also about flow separation and its impact on the performances of an airfoil. A quick overview of air flow control strategies is presented and a literature review about continuous blowing studies is performed.

2.2 Reminder about airfoils and forces convention

An airfoil is a shape representing the cross section of a wing (aircraft) or a blade (helicopter, turbine, turbocompressor). It is a usually slim object with various camber and thickness (see figure 2) whose goal is to interact with an air flow (by opposition with an hydrofoil, which is designed to be used in a water flow). The desired effect of an airfoil varies with the application : lift for a aircraft's wing or a helicopter's blade, compression on turbocompressor's blade for example.

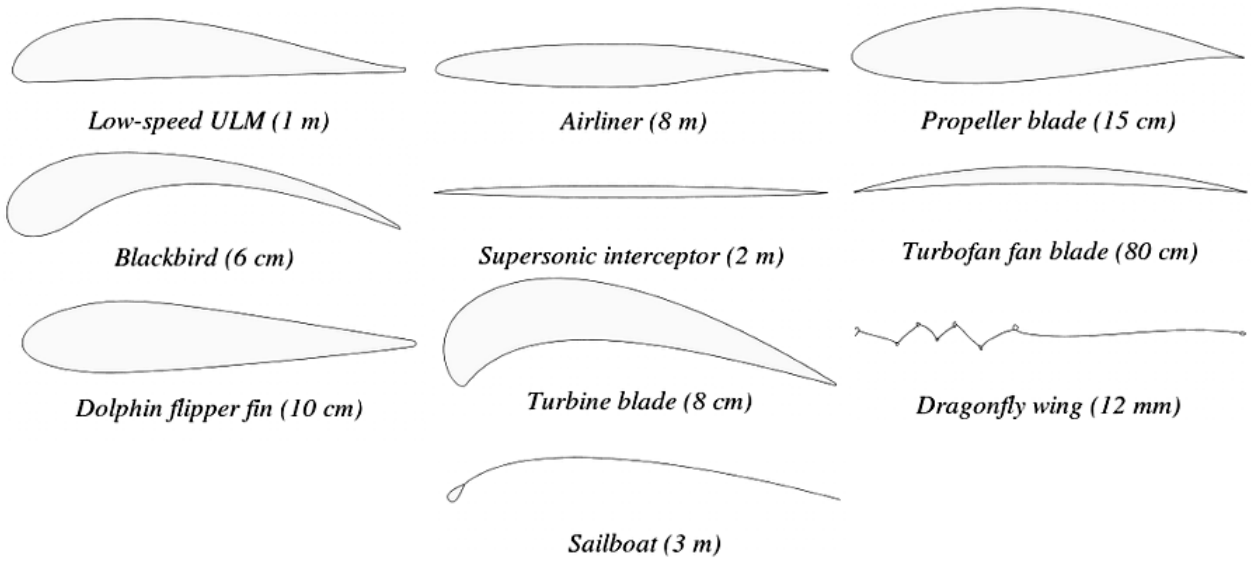

Figure 2: Examples of many types of airfoils

When an airfoil is placed in an flow, we define α, the angle of attack (AoA), as the angle between the chord of the airfoil, which is define as the line joining the leading edge and the trailing edge, and the direction of the inflow "wind". The upper (resp. lower) surface of the airfoil is called the suction (resp. pressure) side, and the camber line is defined as the line situated at the half thickness of the airfoil (see figure 3).

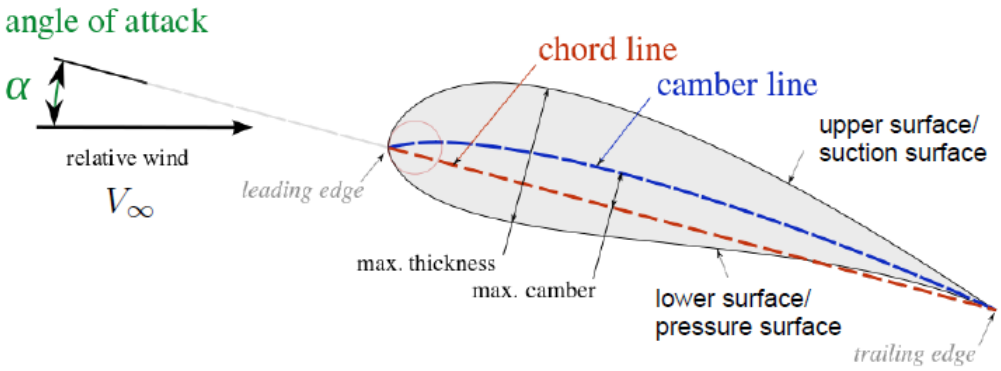

Figure 3: Description of an airfoil

The flow developing around an airfoil produces a force on it. This force is, by convention, decomposed into two components :

- The component perpendicular to the inflow velocity is called the lift. It is produced by a difference in pressure between the suction and pressure sides. The production of this force is the main purpose of a wing to be able to carry an aircraft in the air.
- The component aligned with the inflow is called the drag. There are two types of drag which add with each other but come from different sources : First, the skin friction drag is produced by the diffusion of momentum of the flow, through the boundary layers, to the airfoil. Secondly, the pressure drag is the resulting force induced by the pressure distribution on both side of the airfoil. When the

These two forces are made dimensionless, as it is usual in aerodynamics, into the lift and drag coefficient, using the dynamic pressure of the inflow and the reference surface of the airfoil :

$$C_L \triangleq \frac{L}{\frac{1}{2}\rho_\infty . V_\infty^2 . S} \tag{1}$$

$$C_D \triangleq \frac{D}{\frac{1}{2}\rho_\infty . V_\infty^2 . S} \tag{2}$$

2.3 Physics of airfoil flow separation

In a flow, the fluid particles are subjected to different forces which affect their movement. Firstly, the pressure forces accelerate (resp. decelerate) the particles when the particle faces a negative (resp. positive) pressure gradient. Secondly, the viscous forces, coming from the molecular viscosity, tend to diffuse the momentum from fast to slow particles. When we study a flow close to a wall, the viscous forces diffuse the momentum to the wall, where the velocity is null, resulting in a boundary layer whom thickness grows over the surface as the flow loses some of its momentum. This induces a shear friction on the wall, proportional to the velocity perpendicular gradient evaluated on the boundary (see equation 3).

$$\tau_w = \mu \left. \frac{\partial u}{\partial y} \right|_{wall} \tag{3}$$

If a negative pressure gradient is present above a wall, its induced force will compensate the viscous forces and the boundary layer thickness will remain low over the surface (or even be reduced) as the flow is accelerated. If the pressure gradient is positive, like when a subsonic flow faces a divergent

wall, its effects will add with the viscous forces, and the boundary layer will progressively grow until the velocity normal gradient at the wall becomes zero. This point is called the separation point which have a zero friction coefficient, and the flow is then said to be separated as the flow lines leaves the wall's vicinity. Methods has been developed to try to compute the position of this separation point on airfoils (Twaithe's method, Falkner-skan solutions for boundary layers, Head's method, Stratford's method, to name some [4]). Behind the separation point, the adverse pressure gradient continues to reduce the already low velocity, creating a recirculation zone.

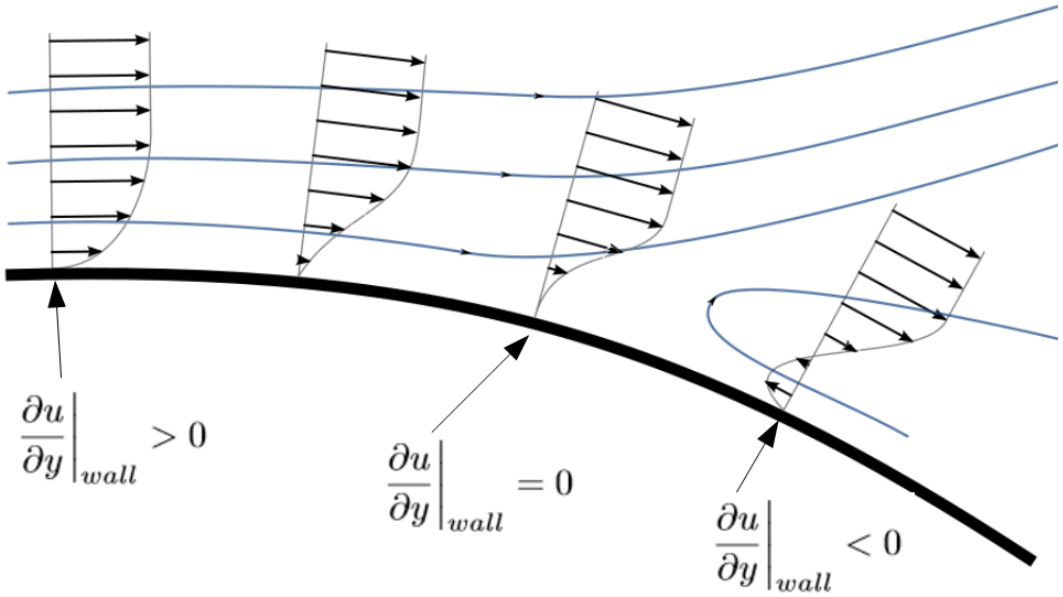

Figure 4: Illustration of the flow separation and recirculation phenomenon

On aircraft, flow separation can occurs on the suction side of the wings when the angle of attack is high as the flow faces an adverse pressure gradient. This behaviour is critically dangerous for the safety of the aircraft as the lift produced by the wings drops drastically and is not high enough to keep the aircraft in the air. Beyond a critical angle of attack depending on the airfoil, the aircraft is said to be stalling. The figure 5 shows a typical lift curve of an airfoil with no camber. One note that it is the lift coefficient that presents a maximum when the angle of attack is growing. At the same AoA, an airfoil will produce higher lift and drag forces when the inflow velocity V_∞ is higher, as the equations 1 and 2 show it.

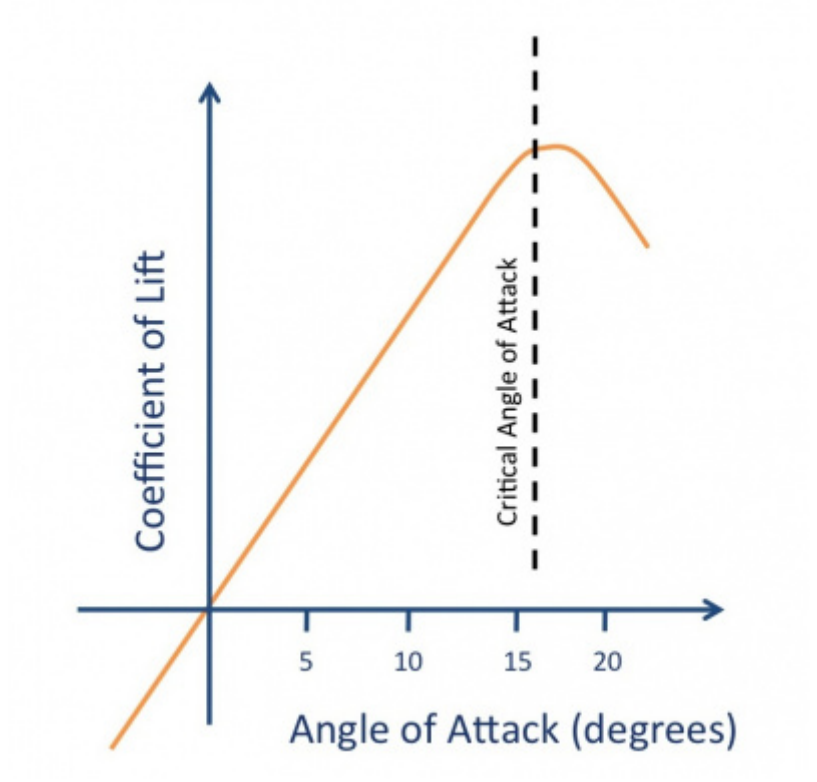

Figure 5: Illustration of a typical lift curve of an airfoil, with the stall point

2.4 Air flow control strategies

For an aircraft to fly, its wings must produce enough lift to compensate its weight. During the take-off and the landing phases, the velocity of airliners are usually low, and the required angle of attack for the wings to produce enough lift is larger than the critical AoA : the aircraft would stall. To allow airliners to fly, techniques can be used to enhance the maximum lift coefficient by delaying the flow separation on the wings at high angles of attack. These are the air flow control actuators that can also be used to provide benefits other than the enhancing of the lift (reduction of wake vortices, reduction of skin friction drag, reduction of noise). They are split in two categories :

- Passive flow controls actuators are modifications applied to the wings construction that does not require any kind of energy input to produce benefits. Some examples are the riblets, fences and vortex generators (see figure 6).
- Active flow control (AFC) actuators are methods that require an input of energy to act on the flow. There are multiple types of AFC (mechanical, plasma, electromagnetic, fluidic) and I will not explain in details all of them (one can refer to [2] to obtain more information about AFC types). The high lift devices (HLD) are a widely used AFC strategy which delays the flow separation, and allow airliner's wings to produce more lift during take-off and landing phases (see figure 8). These HLD are deployed and retracted at will by the pilots, and a power source is thus required, as they must overcome large aerodynamic forces.

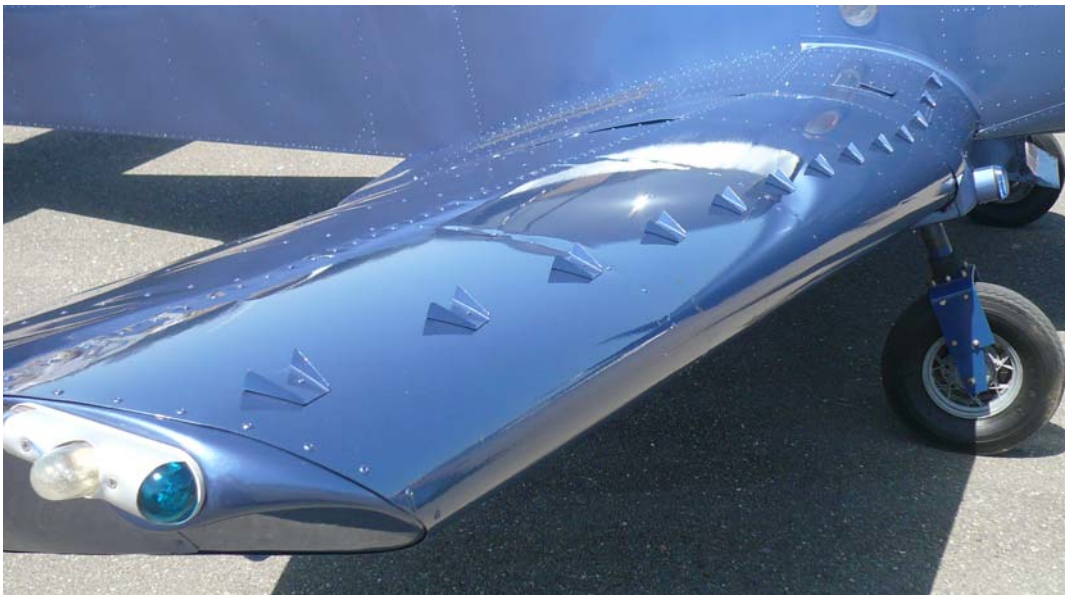

Figure 6: Example of passive air flow control actuator : Vortex generators on a Zodiac CH 601 HD wing

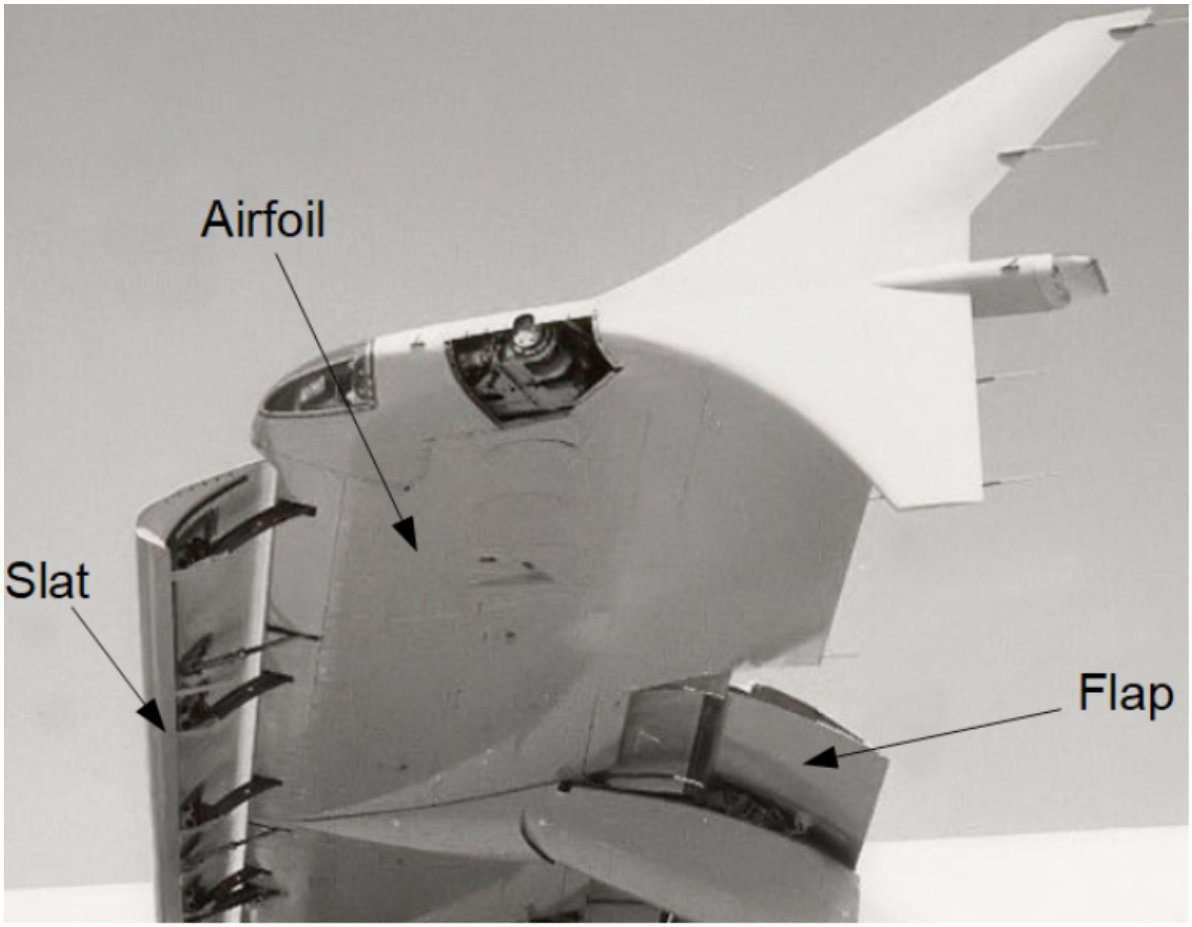

Figure 7: Example of active flow control actuator : high lift devices on an airliner

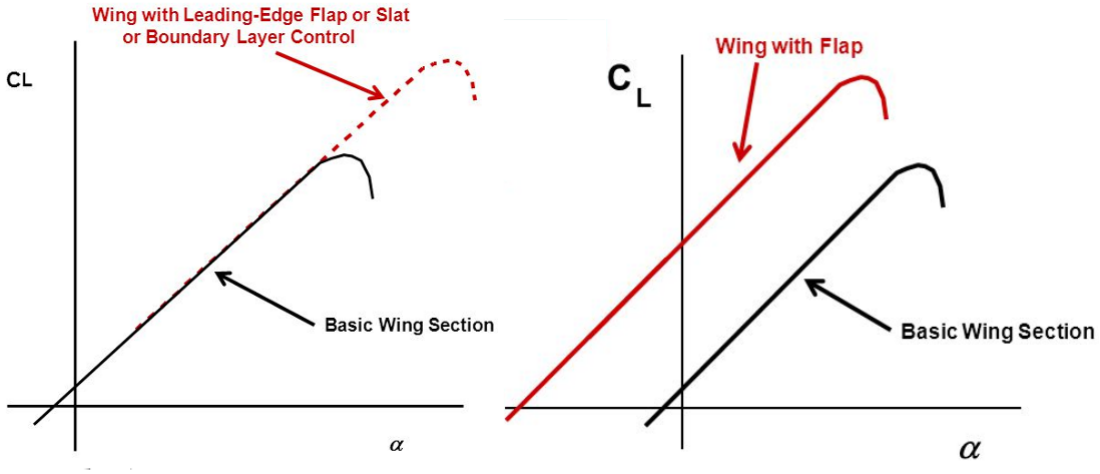

Figure 8: Schematic of the impact of the high lift devices on the lift coefficient of a wing

During the last decades, new types of AFC control as been studied and tested on airfoils.Their technology readiness level is not yet high enough to be integrated on commercial aircraft. The type of active AFC studied in this thesis is a fluidic actuator, which means that a high-momentum fluid is injected in the external flow to re-energize the boundary layer on the suction side of an airfoil. This allow to delay the flow separation, and enhance the performances of the airfoil at high angles of attack and low velocities.

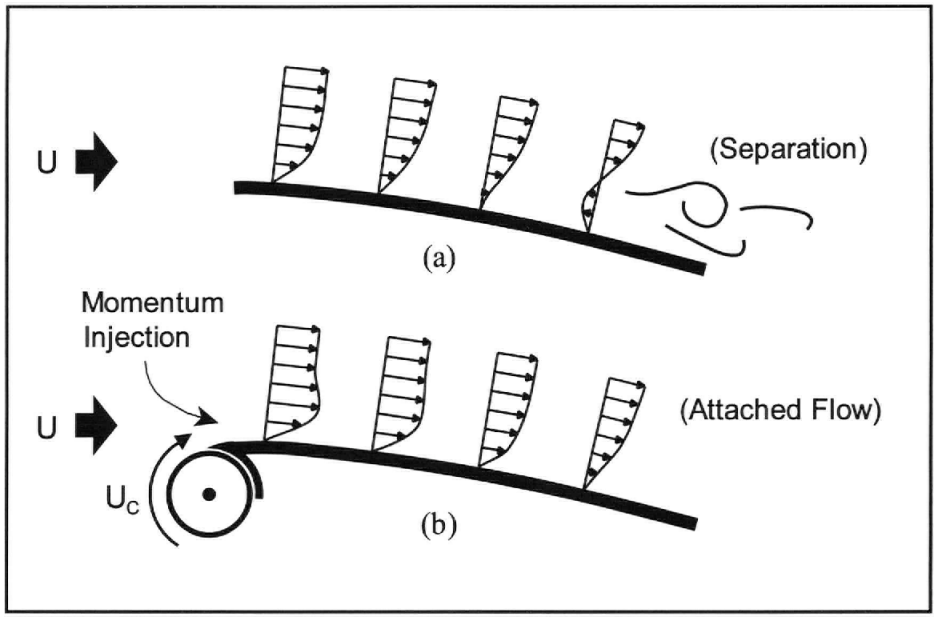

Figure 9: AFC actuator : blowing in the boundary layer

2.5 Literature review

In this section, a review of the literature about AFC using continuous blowing is performed.

- [5] Tadjfar and Asgari : They performed the CFD analysis of an NACA0012 airfoil at Re = 1.10^6 with a continuous blowing close to the leading edge. They obtained a drag reduction of up to 80% and observed that placing the injection slot just upstream of the recirculation vortex has great benefits on the lift and drag.
- [6] Hue and al. : They used CFD (RANS) to simulate an aircraft in a realistic high-lift configuration to study a continuous injection at the engine/wing junction. They performed a comparative analysis on different parameters (slot size, injection velocities) and provided the lift polar. They obtained that flow separation is delayed by one or two degree compared to their baseline.
- [7] Gebhardt and Kirz : They investigated the impact of continuous blowing on the side force coefficient of a rudder. A configuration with a continuous slot and one with multiple discrete slots are studied and compared. The results are that multiple slots at higher jet velocity are better than a continuous slot (at constant increase in side force coefficient).
- [8] Kühn and al. : They performed a 3D CFD (RANS) analysis of an aircraft in high lift configuration, with massive flap separation on the suction side of the flap, and implemented a continuous blowing control. They demonstrated that the flow separation can be suppressed thanks to the energy added to the flow by the blowing.
- [9] De Giorgi. and al. : They made the analysis of a NACA0015 airfoil and a compressor stator cascade with two kinds of AFC : a continuous blowing and a synthetic jet actuator. They concluded that AFC using these actuators is effective to inhibe the flow separation and that the synthetic jet provides better benefit at a same momentum coefficient.
- [10] Chen and al. : They studied the application of a blowing over an elliptical airfoil and analyzed the effect of multiple factors such as the slot width, location and orientation, and the momentum coefficient of the blowing. They obtained that the position of injection plays a large part in the effectiveness of the AFC when it is close to the natural point of separation. For narrow slots, they concluded that the lift increment scales mostly with the momentum coefficient while, for larger slots, the slots width must be considered as an additional parameter.
- [11] Prakash and al. : They implemented an AFC with continuous blowing and suction on a 2D NACA2412 airfoil at Re = $3{,}1.10^6$ using the software OpenFOAM. The turbulence is modelized by the RANS approach with the k-k_l-ω model, and the flow was computed as incompressible. They investigated the influence of the slot location, velocity ratio, angle of perturbation and slot width of both types of AFC. They concluded that low velocity ratios are detrimental to the performances of the airfoil and that best perfomances for the blowing are obtained by locating the injection slot close to the natural separation point of the airfoil. An optimal blowing angle of 30°was also observed.

3 Methodology and modelization

3.1 Introduction

In this chapter, generalities about the numerical computation of fluid dynamic are presented to understand the tools that are used in this thesis to analyze the impact of the AFC system. The models (geometry and mesh) used to simulate the NACA23012 airfoil, with and without control, are described. The physics and boundary conditions are also presented, and a model for the estimation of the power cost of the continuous blowing is provided.

3.2 The CFD Tool

The dynamic of a fluid is governed by the Navier-Stokes equations which express the continuity of mass (equation 4, in conservative form) and the balance of momentum, following Newton's law (equation 5, idem) on a continuous medium. In a case of a compressible flow ($\rho \neq$ cst), a third equation is added to express the balance of energy, and a state law is required to link the pressure, the density and the temperature of the fluid. The air, for example, is usually assimilated to a perfect gaz, whose state law is recalled by the equation 7. For incompressible flows, the dynamic is not affected by the temperature (given the hypothesis of constant viscosity and without the Boussinesq's approximation), and the mechanical problem is decoupled from the thermal problem, which can thus be solved apart.

$$\frac{\partial \rho}{\partial t} + \nabla \cdot (\rho \mathbf{u}) = 0 \tag{4}$$

$$\frac{\partial (\rho.\mathbf{u})}{\partial t} + \nabla \cdot (\rho.\mathbf{u} \otimes \mathbf{u}) = \nabla \cdot \sigma + \rho \mathbf{g} \tag{5}$$

$$\frac{\partial (\rho.U)}{\partial t} + \nabla \cdot (\rho.\mathbf{u}.U) = \sigma : \mathbf{d} + \mathbf{r} - \nabla \cdot \mathbf{q} \tag{6}$$

$$\frac{p}{\rho} = R.T \quad ; \quad U = c_p.T \qquad \text{where R} = \frac{\mathcal{R}}{M_m} \tag{7}$$

These are non linear and parabolic partial differential equations which can only be analytically solved on very simple geometries and cases. Today, computation of fluid dynamics (CFD) is intensively used in lot of industrial fields (aeronautics, automobile, chemistry, etc). Numerical methods to solve the N-S equations on complex geometries have thus been developed to perform numerical studies, allowing investigations that couldn't be done before without building expensive, on scale prototypes.

The turbulent behaviour of practical flows plays a large part of the difficulty of obtaining an accurate numerical solution of the N-S equations, because of unsteady vortex produced at different length scales. There are three different approaches in CFD to capture these eddies and produce accurate simulations :

- The Direct Numerical Simulation (DNS)
  DNS approach completely solves the N-S equations : all the turbulent structures of the flow, from the largest to the smallest vortex, must be computed to obtain the accurate solution of the flow. Since the smallest vortices are at the order of the Kolmogorov's scale, $\eta = (\nu^3/\overline{\epsilon})^{1/4}$ (where $\overline{\epsilon}$ is the turbulent energy dissipation rate), the smallest element of the mesh must be at this scale too, resulting in a huge number of elements and thus in a huge computation time. For this reason, DNS approach is not suited for industrial applications but better for academic purpose as they can provide accurate data that can be used to developed models of turbulence.

- The Large Eddy Simulation (LES)
  LES approach uses a low-pass spatial filter on the N-S equations to avoid the computation of the smallest turbulent structures in the flow while the larger ones are still computed. The small eddies that are filtered away are still modelized to provide accurate solutions. This approach requires less computation time than the DNS and allow unsteady solutions to be computed for many practical cases in a reasonable time.

- The Reynolds Averaged Navier-Stokes equations (RANS)
  The RANS approach solves the time-averaged N-S equations : all scalar and vectorial quantities are decomposed into their average values, with low frequency, and higher frequency fluctuating components (known as the Reynolds decomposition, see equation (8). Introduced in the N-S equations, they are then time-averaged to obtain the RANS equations which are ultimately solved on the desired geometry. In this approach, turbulence is fully modelized, allowing much coarser mesh and a acceptable computation time at the detriment of accuracy, but also of the possibility to simulate unsteady cases : only the averaged quantities are computed. Nevertheless, the majority of commercial CFD software use the RANS approach as it allows fairly accurate results with the fatest computation time of all approaches. Different models exist for the computation of turbulence and are variably accurate depending on the studied type of flow.

$$\phi_{(\mathbf{x},t)} = \overline{\phi}_{(\mathbf{x},t)} + \phi'_{(\mathbf{x},t)} \tag{8}$$

The CFD analysis presented in this thesis is performed using the commercial CFD software ANSYS Fluent which allows to build complex geometries, then meshes them and finally uses the RANS approach to compute the steady flow solution, with the desired boundary conditions. Any field or quantities of interest can be computed and visualized by the software, providing a excellent tool for numerical investigations. For an airfoil, the lift and drag coefficients can be computed, as well as the velocity and pressure fields.

The goal of this thesis is to evaluate the impact of a specific type of fluidic active flow control (the continuous blowing) on the performances of a NACA23012 airfoil. The problem is assimilated to a 2 dimensions situation, similar to a wind tunnel test, where a wing of constant profile and large aspect ratio is placed in a uniform flow to minimize the edge's effects. The investigation is focused on the behaviour of the boundary layer developing on the suction side of the airfoil as well as on its performances at all angles of attack. An airfoil without any blowing is first built to provide a baseline for the AFC investigation. The quantities of interest that will be studied are : The lift coefficient C_L, the drag coefficient C_D and the dimensionless position of the flow separation $\overline{x}_{sep}$, if any. An airfoil with a blowing channel close to the leading edge is next build and simulated. To compare its performances with the baseline, the same quantities of interest are computed, with the addition of the power required to sustain the blowing, which will be estimated. Multiple configurations of the blowing are simulated to try to optimize the AFC : the several characteristics of the blowing are modified between the simulations to investigate their impact on the performances of the airfoil. These characteristics will be presented in the dedicated section.

3.3 Baseline model

3.3.1 Geometry and mesh

The geometry of the NACA 23012 airfoil is provided by the online tool airfoiltools.com [12] and transposed into ANSYS Fluent as a 2D contour surrounded by a large C-domain which is 25 larger than the airfoil's length (see Fig. 10). This type of domain is very classical in airfoil simulations. A structured mesh is then build on this shape with a finer refinement close to the airfoil and also close to the leading edge (see Fig. 11 and 12) to accurately capture the developing boundary layers on the

suction and pressure sides. The turbulence model that will be used requires a first cell dimensionless height $y^+ < 1$ so that it is accurate. An estimation using the Schlichting skin-friction correlation [13] evaluates that the first cell height must have a maximal value of $\Delta y = 5{,}3.10^{-6}$ [m]. The table 1 shows the relevant properties of the resulting mesh quality.

Baseline mesh properties	
Number of elements	307 000
First cell height	$5{,}0.10^{-6}$ [m]
Number of nodes on the airfoil	1100
Grow ratio, close to the airfoil	1,05
Airfoil chord	1 [m]

Table 1: Baseline mesh properties

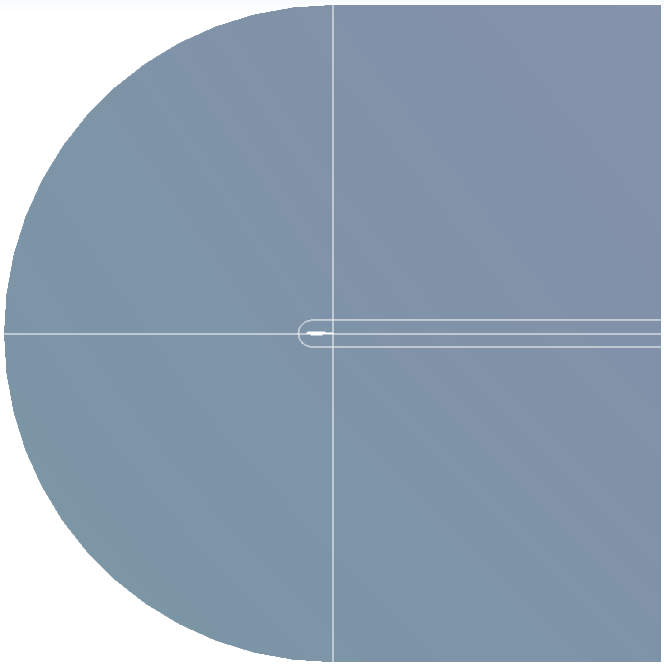

Figure 10: Geometry of the baseline's domain of computing

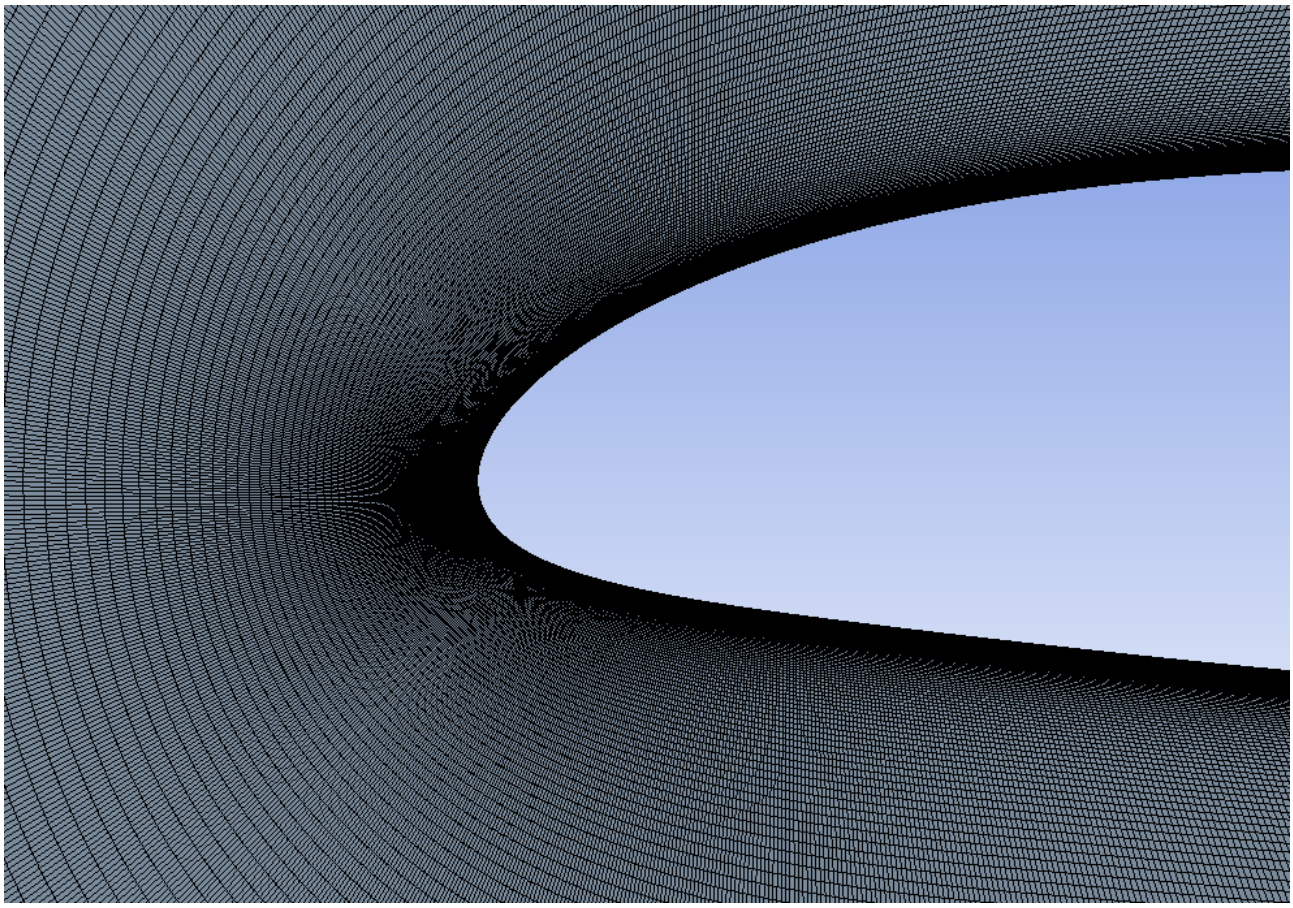

Figure 11: Closer look at the mesh around the baseline NACA23012 airfoil's leading edge

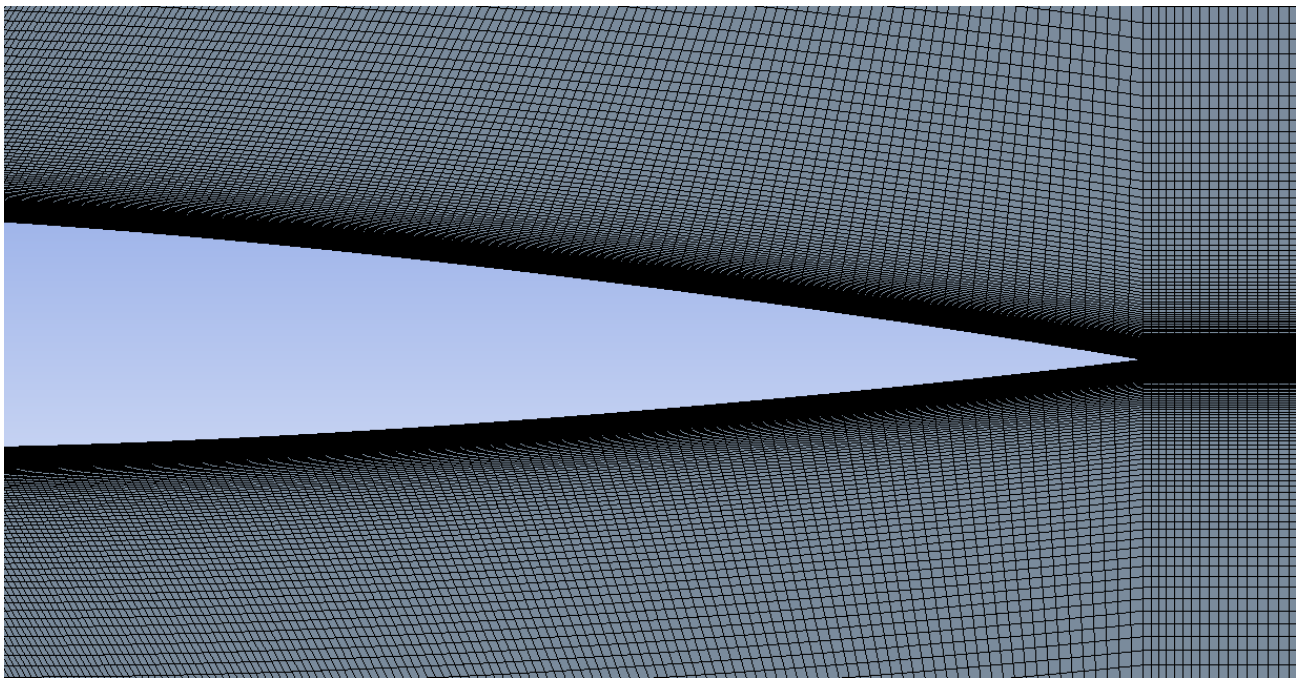

Figure 12: Closer look at the mesh around the baseline NACA23012 airfoil's trailing edge

3.3.2 Problem definition and models choice

The baseline study is performed on an airfoil at low speed and standard atmosphere (conditions similar to the take-off and landing phases of an aircraft). The table 2 shows the inflow conditions used for the baseline but also for the further analysis about the continuous blowing. Once the mesh is built on the geometry, the computation models and the boundary conditions are set. The airfoil is solved for a span of angles of attack from -8°to +20° by steps of 2° (with an additional AoA of 19°) to get the polar of the airfoil. To change the angle of attack, the velocity components of the inflow are modified so that the wind relative to the airfoil is at the correct AoA. The free stream velocity components are easily recovered using equations (9) and (10). The simulations for each AoA are initialized using the computed solution of the previous AoA to minimize the computation time.

$$V_{\infty,x} = V_{\infty}.cos(\alpha) \tag{9}$$

$$V_{\infty,y} = V_{\infty}.sin(\alpha) \tag{10}$$

Inflow properties	
V_∞	76,0 [m/s]
ρ_∞(sea level)	1,177 [kg/m^3]
T_∞ (sea level)	300 [K]
p_∞ (sea level)	101325 [Pa]
Re_∞	5,0.10^6
M_∞	0,222
μ	1,7894.10^{-5} [Pa.s]

Table 2: Physical properties of the free stream

The free stream Mach number is not quite high but the accelerating flow above the suction side of the airfoil can reach high Mach numbers at higher angles of attack and thus a compressible flow must be considered. The perfect gas is used to model the air in standard atmosphere conditions.

As explained before, the turbulence model used in the RANS approach plays a great part in the quality of the simulations. A lot of studies has been conducted to analyze the accuracy of different models for different problems. In this case of computing airfoil flow separation and performances, the k-ω SST model has been proven to be sufficiently accurate [14][15][16].

3.4 Airfoil with blowing

3.4.1 Geometry and mesh

To precisely simulate the continuous blowing, a channel with a length 15 times larger than its width is built and located close to the leading edge of the airfoil. The air injection cannot be perfectly parallel to the airfoil's wall, as it would be too difficult to manufacture, and thus the outlet of the channel is bevelled to an angle (see figure 13). The mesh around the airfoil is generated the same way as the baseline but with a refinement close to the injection slot. A structured mesh is build in the injection channel with a refinement close to its walls, to properly capture the boundary layers, following the same principle as the boundary layers on the airfoil itself. The figures 14 and 15 show the mesh close to the leading edge and injection slot and the table 3 shows the main characteristics of the mesh.

Injection channel mesh properties	
Number of elements	29000
Number of nodes on the walls	230
Number of nodes on the inlet and outlet	100
Grow ratio close to the walls	1,05
Global mesh properties	
Number of elements	466 000
Number of nodes on the airfoil's suction side	1050
Number of nodes on the airfoil's pressure side	450
Grow ratio close to the airfoil's walls	1,05

Table 3: Injection channel mesh, and global mesh properties (airfoil with control)

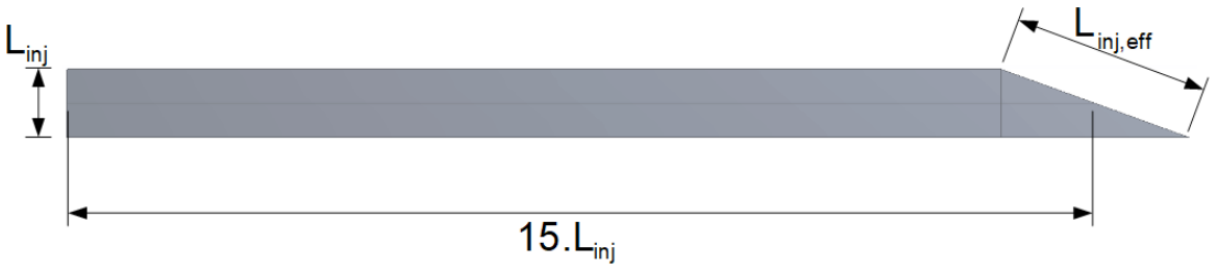

Figure 13: Schematic of the injection slot geometry, with the bevelled outlet

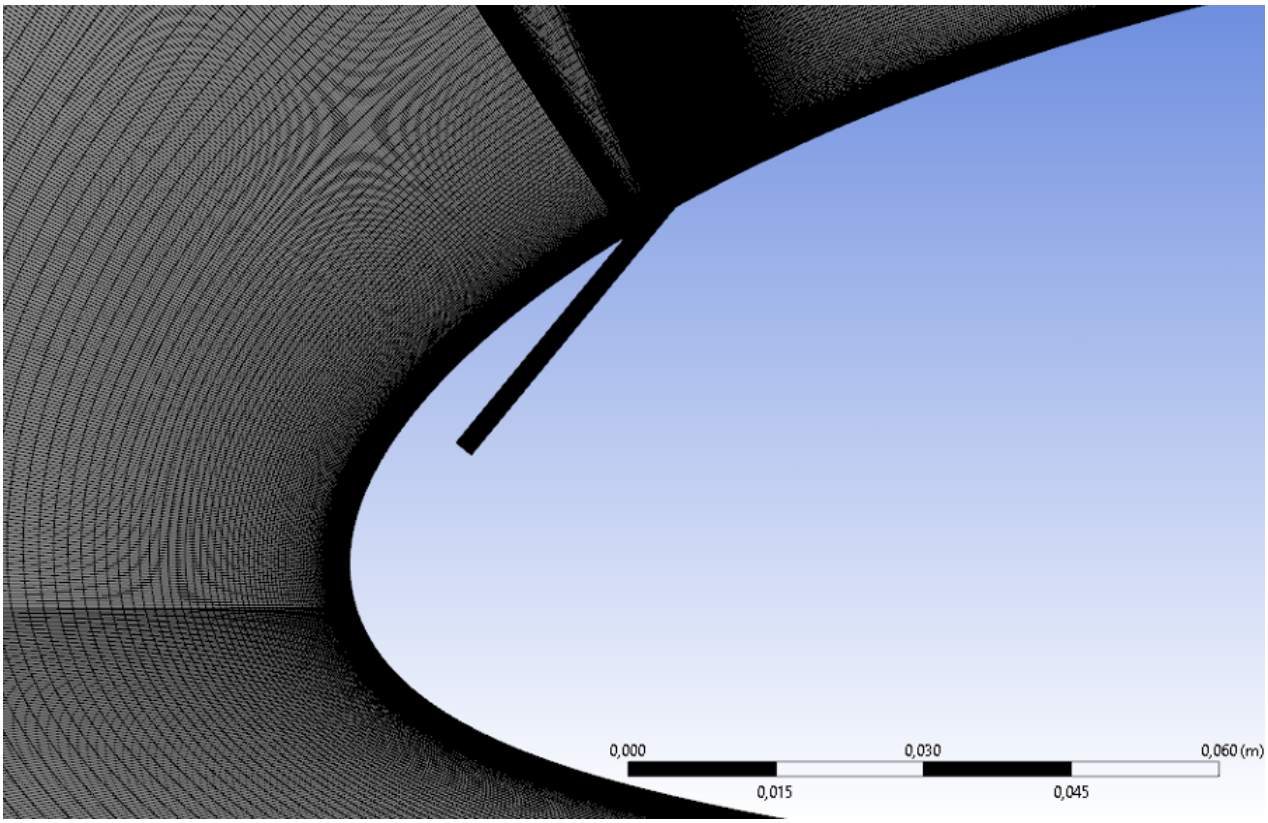

Figure 14: Mesh close to the leading edge of the airfoil with blowing channel

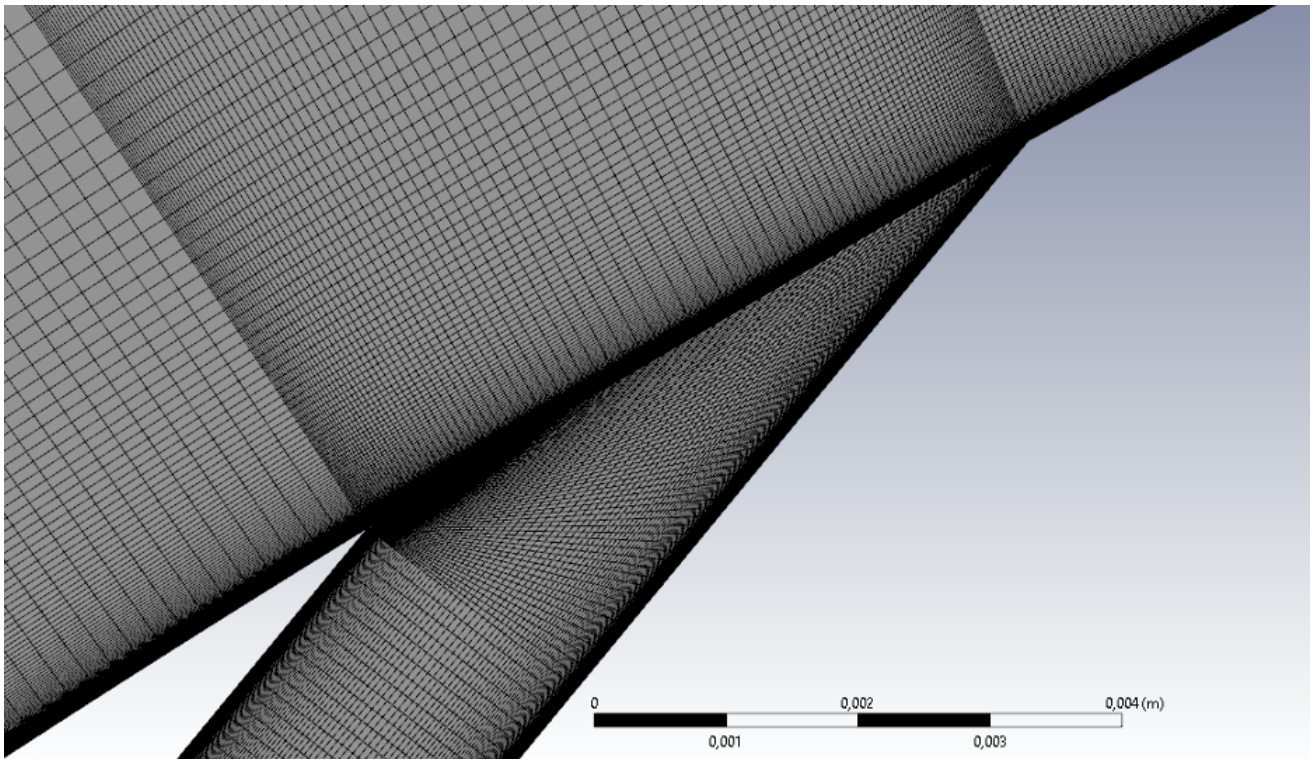

Figure 15: Closer look at the injection slot mesh

3.4.2 Problem definition and models choice

The inflow of the airfoil with AFC system does not change from the baseline. An additional inlet appears with the injection channel. Since the velocity ratio of the blowing will sometimes be quite high, the Mach number will reach high values (while remaining subsonic), and a compressible flow is again considered with the perfect gas model. The k-ω SST turbulence model is also used again. There are two mains different dimensionless parameters which characterize a continuous blowing [17] :

- The momentum coefficient C_μ is the ratio between the momentum flux injected by the blowing system and the momentum flux of the free stream :

$$C_\mu \triangleq \frac{\frac{1}{2}.\rho_{inj}.V_{inj}^2.L_{inj}}{\frac{1}{2}.\rho_\infty.V_\infty^2.c} \tag{11}$$

  This coefficient is a major parameter for the benefices provided by the FC system. High C_μ can be used to control the circulation around the airfoil while low C_μ help to prevent separation of the flow on the suction side of airfoils. Experiments has shown that the transitional values between this two applications are about 3-5%. [17].

- The Velocity ratio VR is the ratio between the velocity of the design actuator flow and a reference velocity, usually the free stream velocity. It must be >1 to be considered high enough to provide benefit to the separation control unless it can still be useful for skin friction drag reduction and transition control [18].

$$VR \triangleq \frac{V_{inj}}{V_\infty} \tag{12}$$

Different configuration of the continuous blowing are investigated. The momentum coefficient and the velocity ratio are linked with each other as they share the injection velocity magnitude. Here is the

steps to build a configuration of the blowing : the channel's width is set, then a momentum coefficient is chosen, and the velocity ratio is adapted so that the definition of C_μ is verified. Too high values of VR are excluded, as they would be too close of supersonic conditions.

3.4.3 Estimation of the power required for the blowing

The main objective of an AFC system on a wing is to enhance the performances of the airfoil while reducing the global cost of the aircraft. The difference with passive flow control is that AFC requires input power to be operational. An estimation of the required power is thus needed to assess its effectiveness. The present AFC consists of injecting pressurized air in a channel in a continuous manner. The behaviour of the flow inside the channel is part of the numerical simulation but the upstream conditions are to be modelized. The figure 16 shows a schematic of the model used.

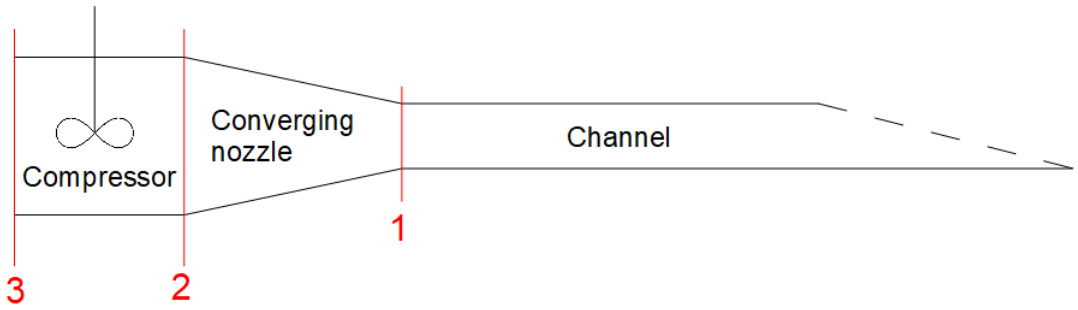

Figure 16: Schematic of the model used to compute the power cost of the injection

The state 1 describes the flow at the entrance of the injection channel, the velocity magnitude is imposed by the wished velocity ratio of the current configuration, and the static temperature is set to $T_1 = 300$ [K]. The static pressure is different for each configuration of the airfoil and of the blowing, and is thus recovered after each simulation. To achieve this inlet flow with high velocity, a converging nozzle is assumed to bring the flow from a state 2, at rest, to the state 1. Since the flow is accelerating, the boundary layers on both side of the channel are supposed to be shrunk to have no thickness at state 1. The acceleration is supposed to be isentropic and the following relationships can thus be written :

$$M_1 = \sqrt{\gamma.R.T_1} \qquad \text{where R} = \frac{\mathcal{R}}{M_m} \tag{13}$$

$$p_{t,1} = p_{t,2} = p_2 = p_1 \left(1 + \frac{\gamma - 1}{2} M_1^2\right)^{\frac{\gamma}{\gamma - 1}} \tag{14}$$

$$T_{t,1} = T_{t,2} = T_2 = p_1 \left(1 + \frac{\gamma - 1}{2} M_1^2\right) \tag{15}$$

$$\rho_2 = \frac{p_2}{R.T_2} \tag{16}$$

The state 2 is a pressurized state at rest, It is assumed achieved after an isentropic compression from the state 3 which is supposed to be at atmospheric pressure. The states 3 is thus computed with the following equations :

$$\rho_3 = \left(\frac{p_3.\rho_2^\gamma}{p_2}\right)^{\frac{1}{\gamma}} \tag{17}$$

$$T_3 = \frac{p_3}{R.\rho_3} \tag{18}$$

The power required to perform the isentropic compression, which is the power cost of the blowing, is finally computed :

$$P_m = \dot{m}.c_p.(T_3 - T_2) \tag{19}$$

We have now an estimation of the power required to sustain the blowing. Of course, a lot of factors interfere with the accuracy of this estimation and is not a precise and definitive evaluation of the power cost of the system.

4 Results and discussion

4.1 Introduction

In this chapter, the results of all configurations of the airfoil, simulated using ANSYS Fluent software, are presented and commented. The polar of the baseline model for the NACA23012 airfoil is shown and the maximum lift angle of attack is identified, and compared to experimental data. A comparative study is then performed to assess the impact of multiple factors relative to the blowing on the performances of the airfoil.

4.2 Baseline results and comparison with experimental data

The figure 17 shows the convergence of the computed lift coefficient using Fluent software, where each flat step corresponds to a certain angle of attack from -8°to +20°by steps of 2°. We see that the first steps (low and intermediate AoA) are quite fast to converge while the last steps (high AoA) take more iterations to converge because of the large flow separation happening on the suction side of the airfoil. The results of the computation of the lift and drag coefficients and the polar of the NACA23012 airfoil are shown on Fig. 18 to 21 where we see that the baseline presents its critical angle of attack before stalling at +16°. Experimental data of the same airfoil from the NASA [19] are also shown on the same figures to compare with the CFD. The NASA performed two set of measurement at a Reynolds number of 6.10^6, one using a usual surface roughness and one with a "standard" roughness which is obtained after a sanding process on the leading edge of the airfoil. The authors consider the resulting roughness to be more severe than usual manufacturing quality or normal use, but less than what can occur in severe conditions (mud or ice accumulation) [19].

The results of the simulations show that the CFD performed here is accurate for the lift coefficient computation (maximum 6% of difference between the CFD and the data) at low and moderate angles of attack. The standard roughness results of the NASA shows lower lift at higher AoA because of the earlier separation resulting of the sanding process. The data of the NASA shows that the surface treatment plays a huge part in the drag coefficient of the airfoil. This is also corroborated by other studies [20] [21] which point out that higher surface roughness increases the skin friction drag but also trigger earlier flow separation. The drag coefficients obtained by the CFD are contained between these two set of experimental data. We conclude that, since it is hard to accurately predict drag coefficients because of factors like surface treatment, and also since the aim of this thesis is not to accurately recover experimental data, the presented results can be used as a baseline for further comparisons with the AFC system. We observe that the maximum lift is achieved at an AoA of 16°.

The Fig. 22 illustrates the CFD at $\alpha = 16°$. We can intuitively see that the flow on the suction side separates near the trailing edge. This is more precisely visible on Fig. 24 which shows the wall shear stress distribution on the suction and pressure sides of the airfoil. As we explained in a previous section, the separation point is defined by the location on the airfoil where the shear stress is zero, which happens at a distance $\overline{x} \approx 80\%$. An other point seems to have a zero shear stress close to the leading edge, this is the separation point where the flow splits around the airfoil (visible on figure 22, where the velocity magnitude is very low close to the airfoil's surface). The figure 23 shows the velocity vectors on the suction side, close to the trailing edge, where we can visualize the recirculation vortex, happening because of the flow separation as we explained in the "Generalities" chapter.

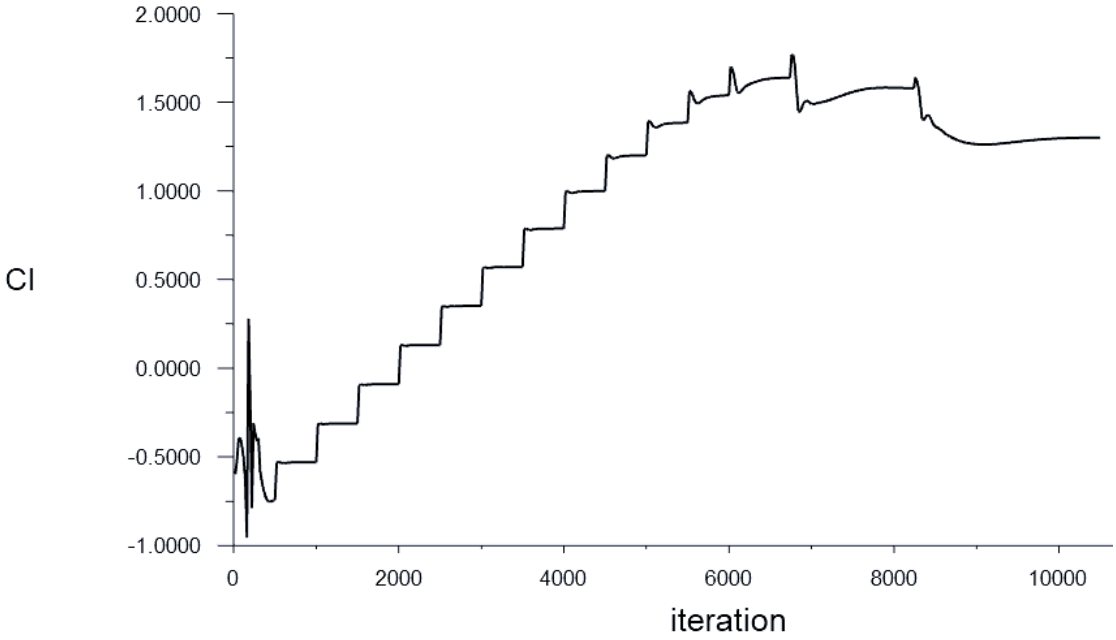

Figure 17: Convergence curve of the computation of the lift coefficient, baseline airfoil

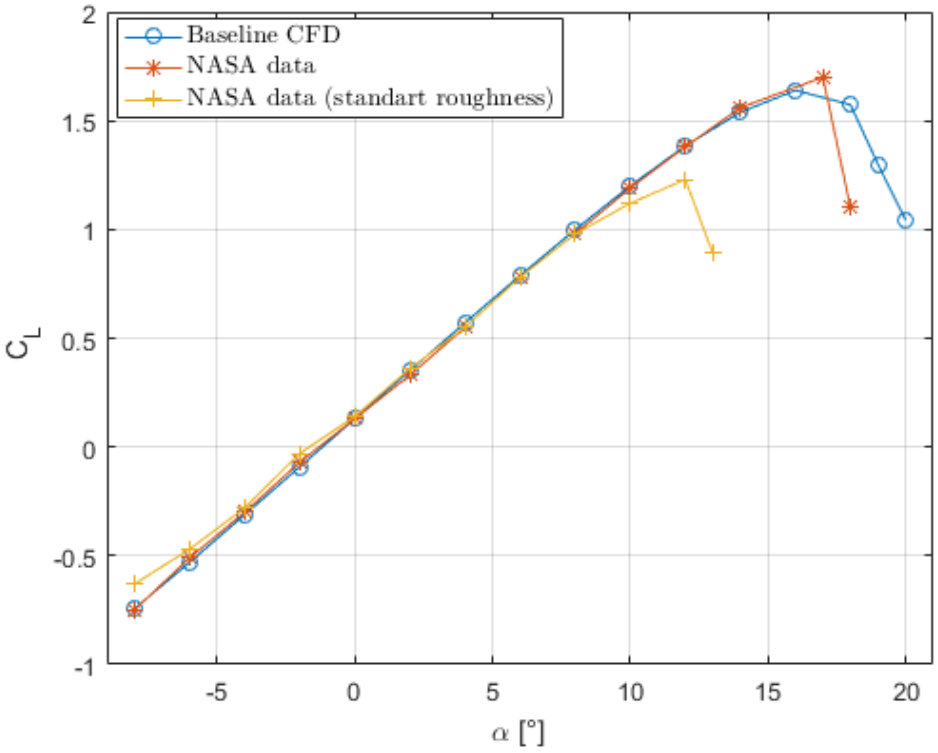

Figure 18: C_L versus α, baseline NACA23012 airfoil

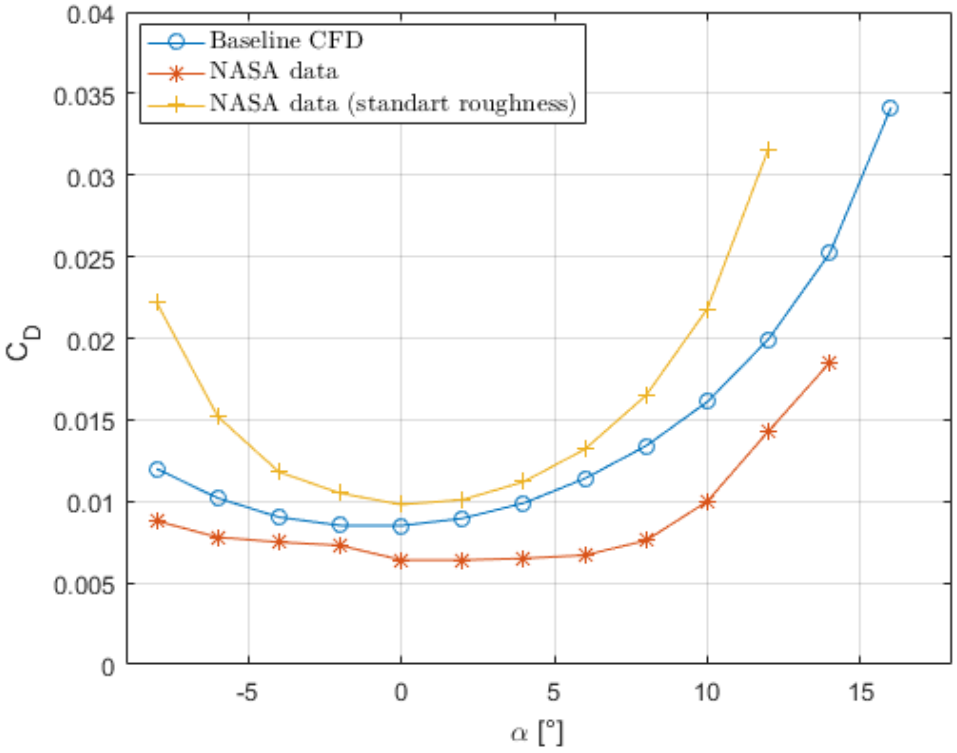

Figure 19: C_D versus α, baseline NACA23012 airfoil

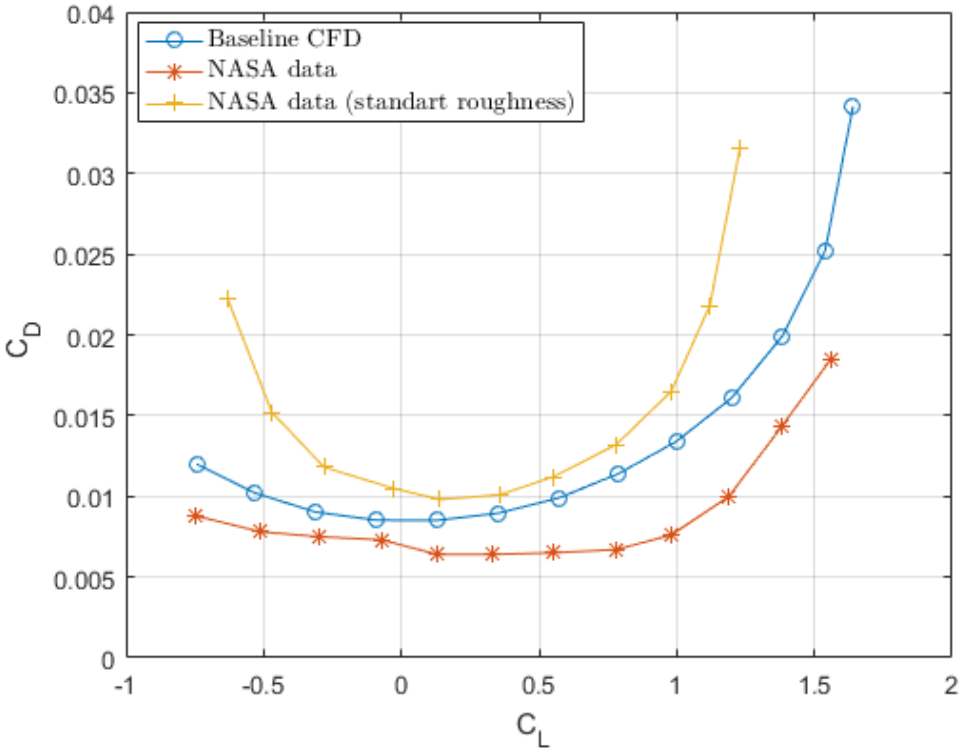

Figure 20: Baseline NACA23012 airfoil polar

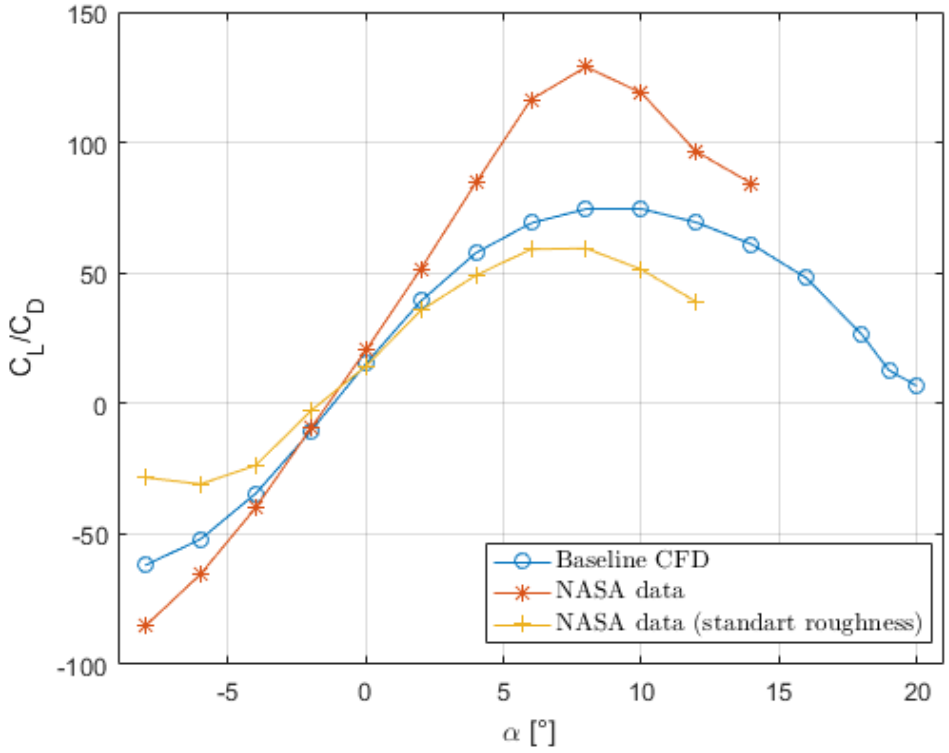

Figure 21: Lift to drag ratio versus α, baseline NACA23012 airfoil

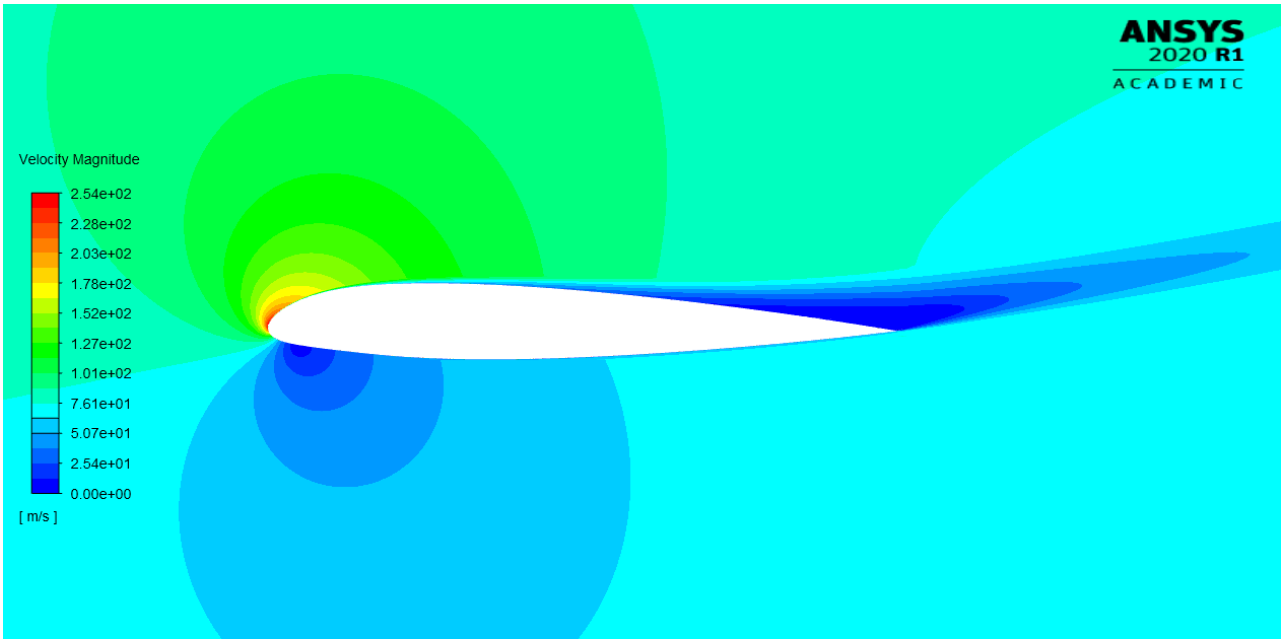

Figure 22: Velocity contour of the baseline NACA23012, $\alpha = 16°$

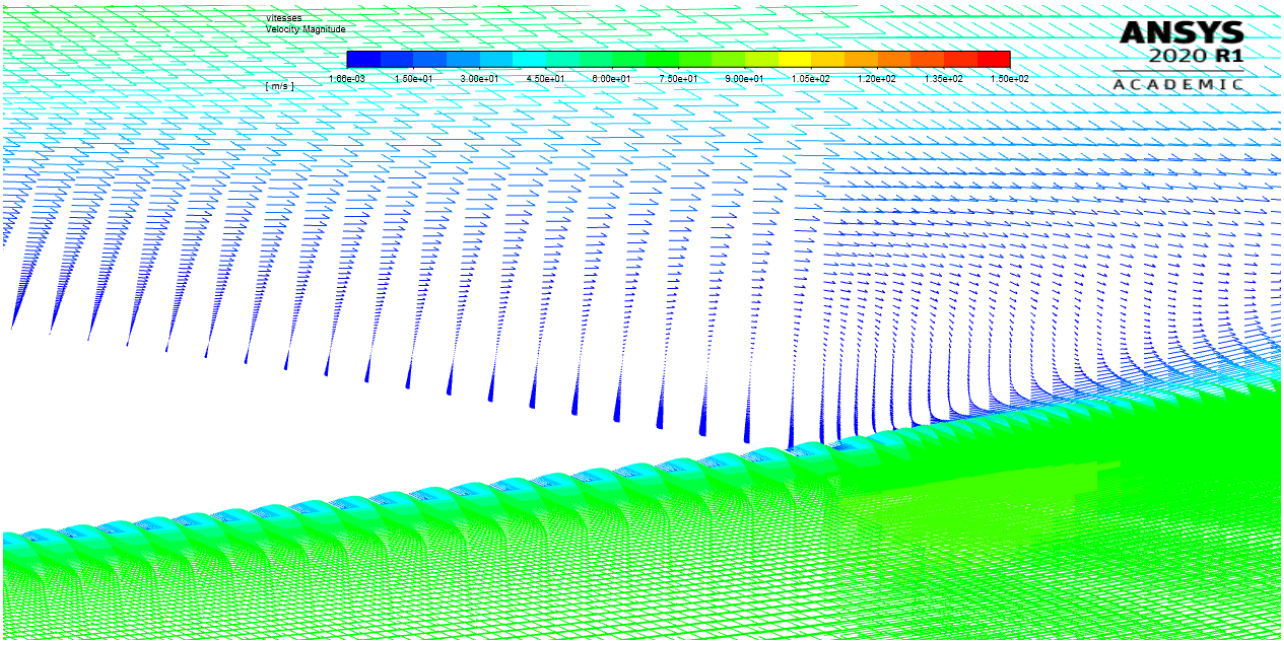

Figure 23: Velocity vectors above the trailing edge of the baseline NACA23012, $\alpha = 16°$

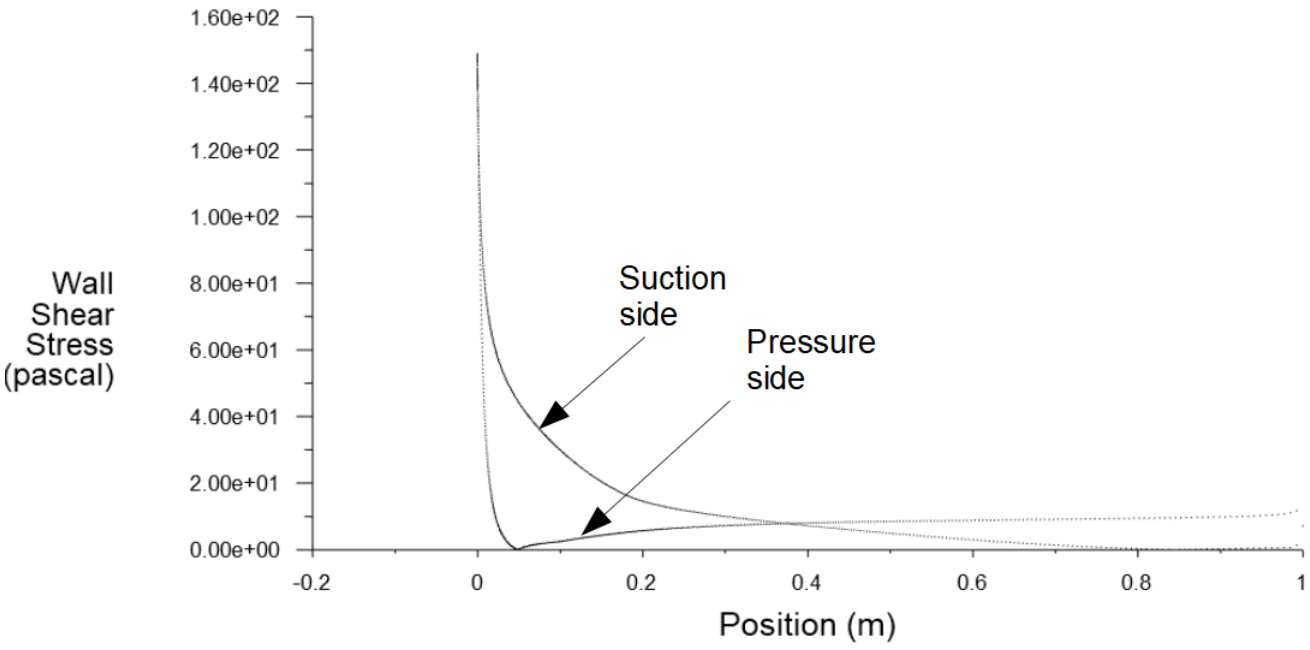

Figure 24: Wall shear stress distribution of the baseline NACA23012, $\alpha = 16°$

4.3 Airfoil with control results

4.3.1 Impact of the momentum coefficient and velocity ratio of the blowing

The first simulated configurations of the airfoil with blowing control aim to evaluate the impact of the momentum coefficient and the velocity ratio. The blowing channel slot is located at a position $\overline{x}_{sep} = 3$ % and the slot is bevelled to an angle of 20°with respect to the airfoil local surface. Different channel widths are used to be able to study different velocity ratios at the same momentum coefficient. At lower widths, the velocity ratios required to achieve higher momentum coefficient is too high to be considered realistic and are thus not simulated. The table 4 shows the different configurations of the blowing computed for this part. All configurations are simulated for a span of angles of attack : 0°, 8°, 12°, 14°, 16°, 18°, 19°and 20°(Sometimes, an additional AoA of 21°is added to observe the stalling behaviour of certain configurations).

	C_μ = 0,5 [%]	C_μ = 1,0 [%]	C_μ = 1,5 [%]	C_μ = 2,0 [%]
L_{inj} = 1,0 [mm]	VR = 2,236	VR = 3,162	-	-
L_{inj} = 1,5 [mm]	VR = 1,826	VR = 2,582	VR = 3,162	-
L_{inj} = 2,0 [mm]	VR =1,581	VR = 2,236	VR = 2,739	VR = 3,162

Table 4: Simulated configurations for the first part

The figures 25 to 28 show the results of the simulations for these different configurations : the lift and drag coefficients are shown regrouped by values of momentum coefficients, and compared with the baseline performances. Here are the conclusions about the performances of the airfoil with control we can extract from these graphs :

- The continuous blowing may not always be useful for enhancing the performances of the airfoil. For a momentum coefficient of 0,5 %, we see that the airfoil with blowing provides actually less lift than the baseline with an earlier stalling, no matter what velocity ratio is used. The loss of performances is not very noticeable at low angles of attack, but becomes important at higher AoA. At C_μ = 1,0 %, the blowing becomes effective at augmenting the performances, but a VR too small (lower than about 2,5) keeps the airfoil at lower performances than the baseline. At higher VR and C_μ, these graphs show that the stalling is delayed by an angle of up to 4°, and that the lift and drag coefficients at $\alpha = 16$°is increased and reduced respectively by up to 23,9% and 18,1% (at the maximal VR and C_μ), compared to the baseline.

- For a given momentum coefficient, higher velocity ratios (which means also thinner injection channel) of the blowing provide better performances to the airfoil. The higher the angles of attack, the larger the differences of performances are. Again, the differences at low AoA are less noticeable than at high AoA.

- At low angles of attack, while the VR does not change the performances too much, the momentum coefficient seems to have an positive impact on the performances compared to the baseline by adding a flat amount of lift which is larger when C_μ rises.

The figures 29 and 30 show the computation of the required power (following the methodology presented in the previous chapter) as function of the angle of attack for different configurations and two momentum coefficients. We see that, for a given C_μ, a higher velocity ratio (which means also a thinner channel) requires more power. Since, as was observed, a larger velocity ratio provides more benefits, higher benefits mean a higher required power. We also observe that higher angles of attack actually reduce the power cost. This can be explained by the fact that the static pressure above the leading edge of an airfoil is reduced when the angle of attack is growing. Since the control injects air in

a lower pressure flow, the pressure upstream of the injection channel is reduced, and so is the required power.

To quantify the effectiveness of the AFC actuator, we can plot the gain of lift of the airfoil with control, relatively to the baseline, versus the required power (see figures 31 and 32). For all configurations, we observe two "branches" : the right branch of each curve (high required power) corresponds to low angles of attack of the airfoil. As we saw before, the control add a flat gain of lift which is large compared to the baseline at low angles of attack (up to 220%, depending on the configuration), but becomes relatively smaller as the AoA rises. The left branch (lower required power) corresponds to higher angles of attack. The large relative gain of lift comes from the earlier flow separation of the baseline, which drastically reduces the lift, and thus increases the relative gain of the control.

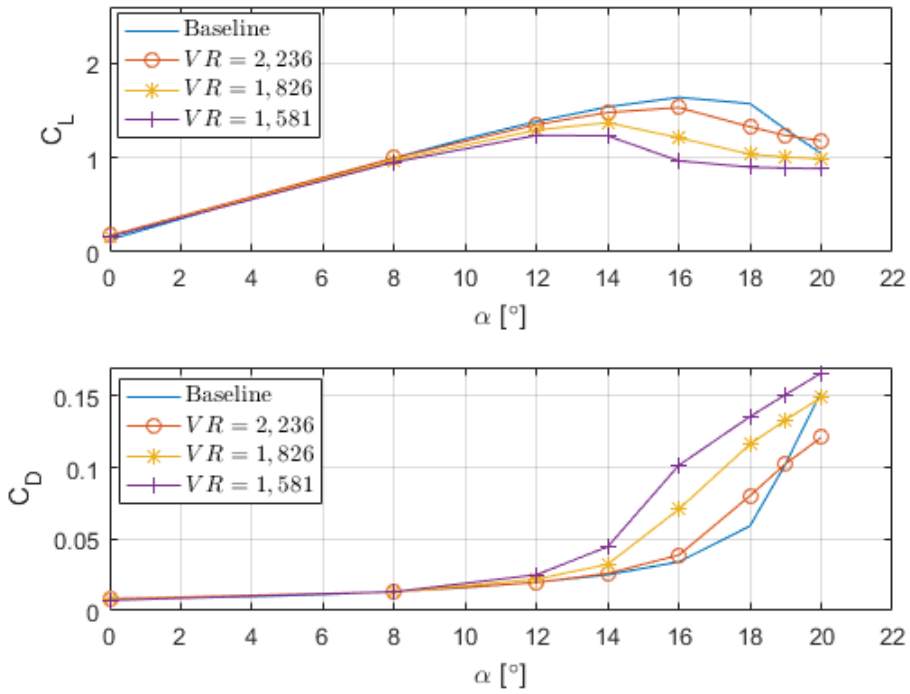

Figure 25: Comparison of the effect of the momentum coefficient and velocity ratio, lift vs α and drag vs α : $C_\mu = 0{,}5$ %

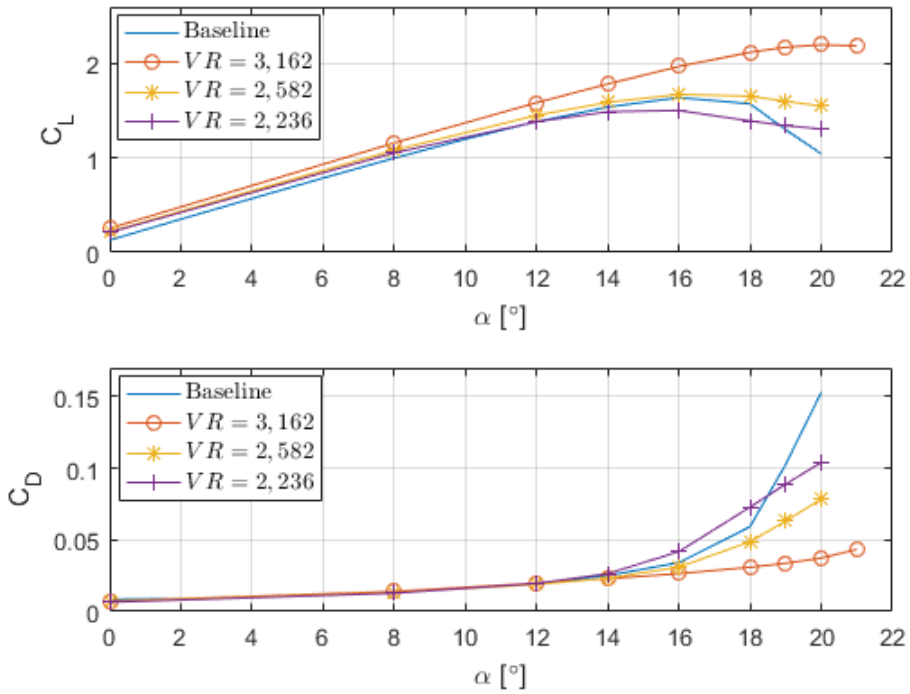

Figure 26: Comparison of the effect of the momentum coefficient and velocity ratio, lift vs α and drag vs α : $C_\mu = 1{,}0$ %

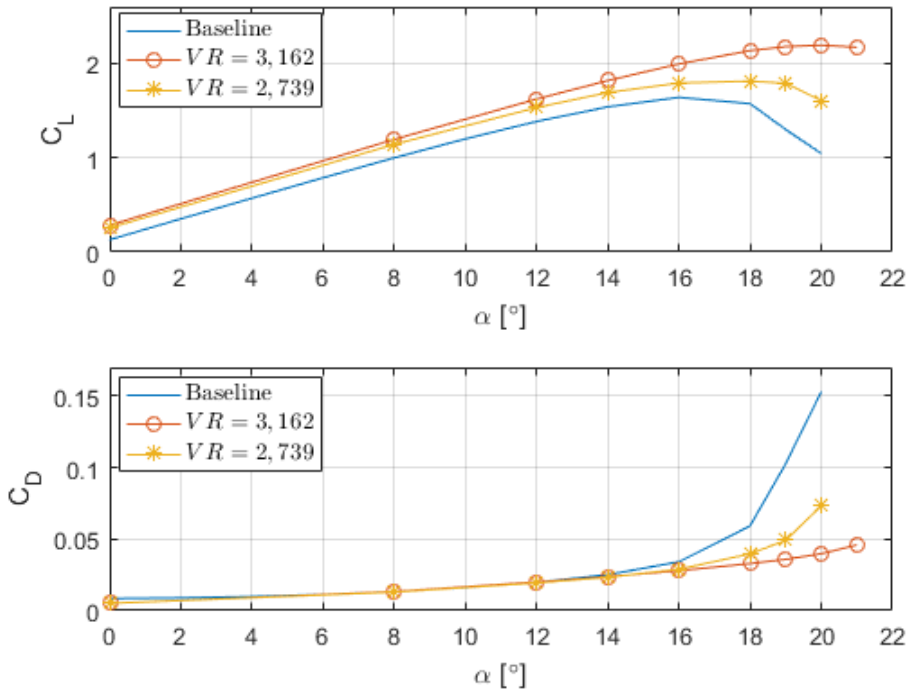

Figure 27: Comparison of the effect of the momentum coefficient and velocity ratio, lift vs α and drag vs α : $C_\mu = 1{,}5$ %

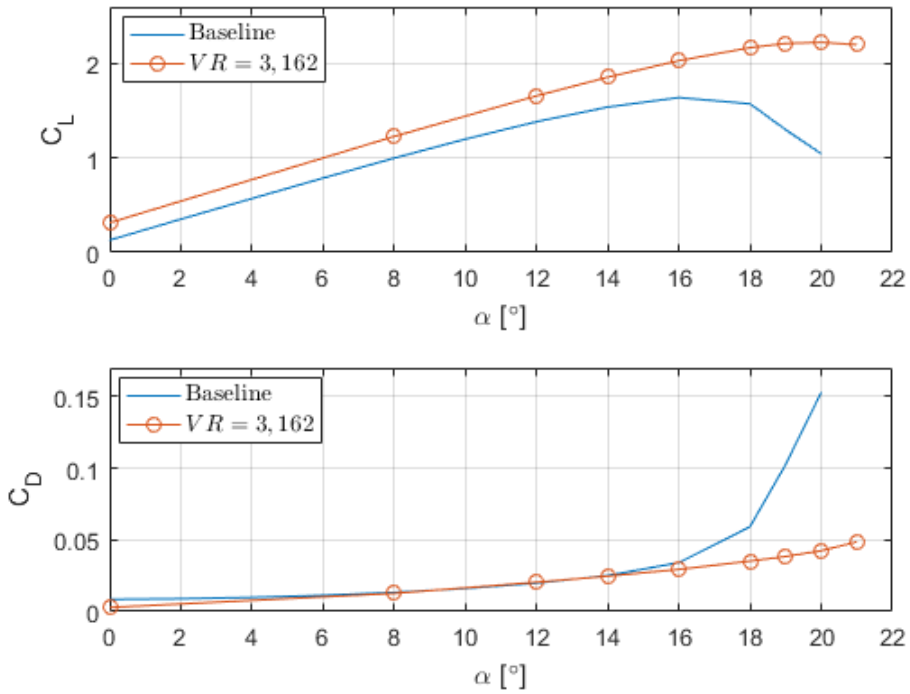

Figure 28: Comparison of the effect of the momentum coefficient and velocity ratio, lift vs α and drag vs α : $C_\mu = 2{,}0$ %

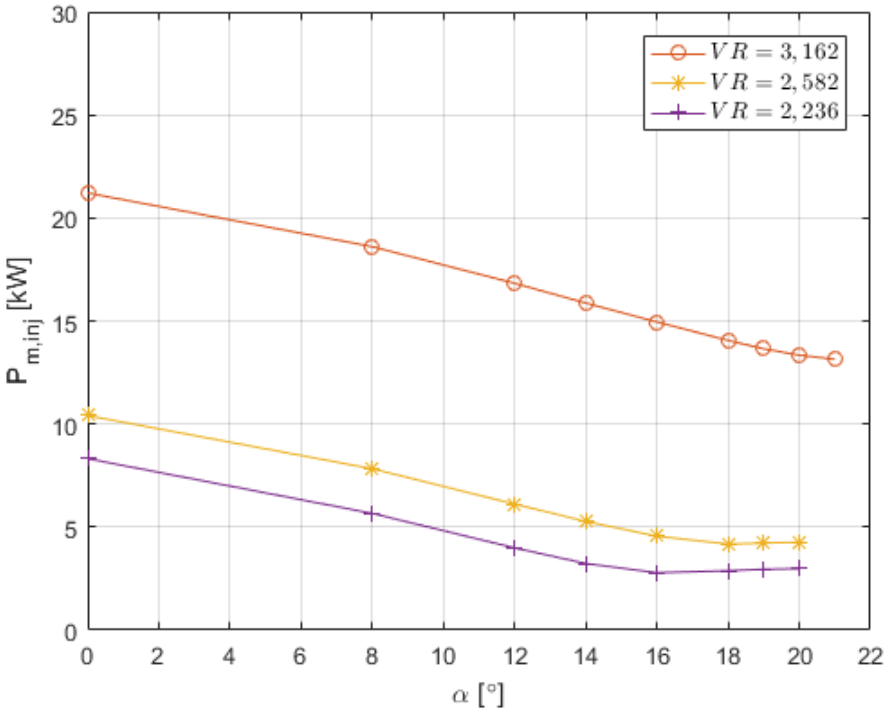

Figure 29: Power required for the control vs α : $C_\mu = 1{,}0$ %

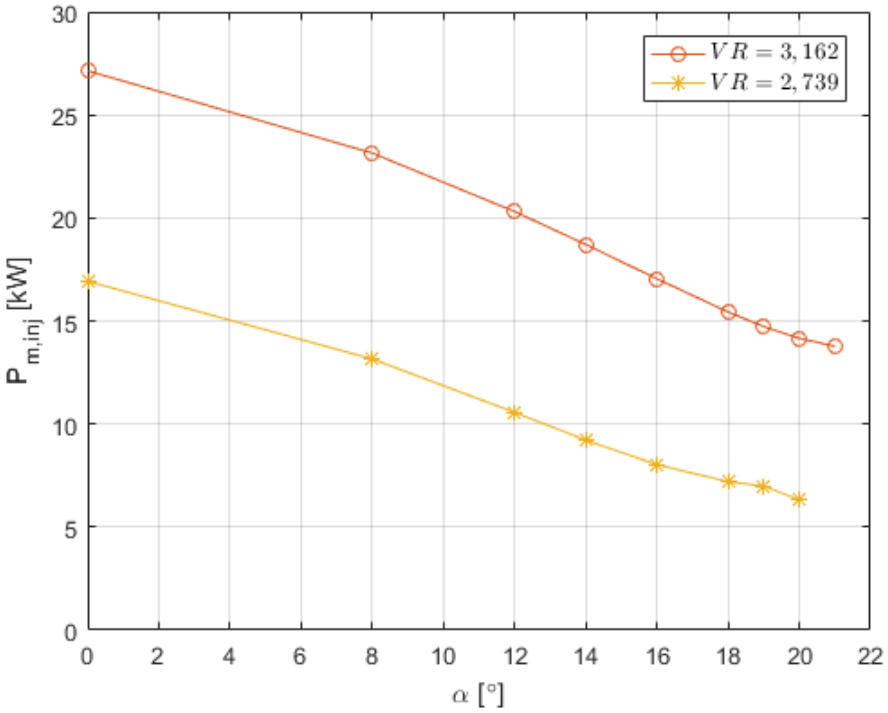

Figure 30: Power required for the control vs α : $C_\mu = 1{,}5$ %

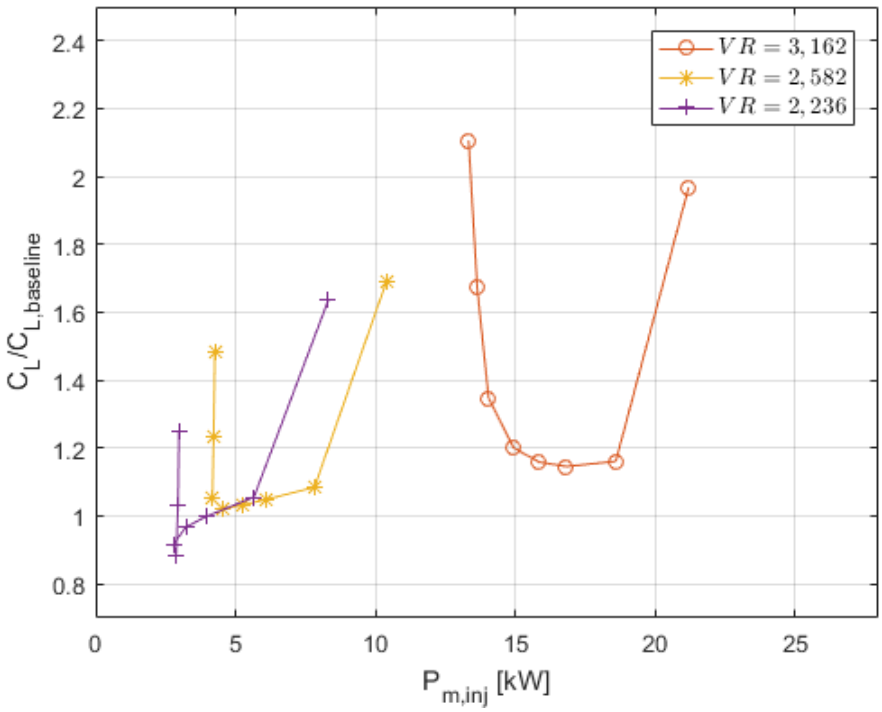

Figure 31: Relative gain of lift compared to the baseline vs required power : $C_\mu = 1{,}0$ %

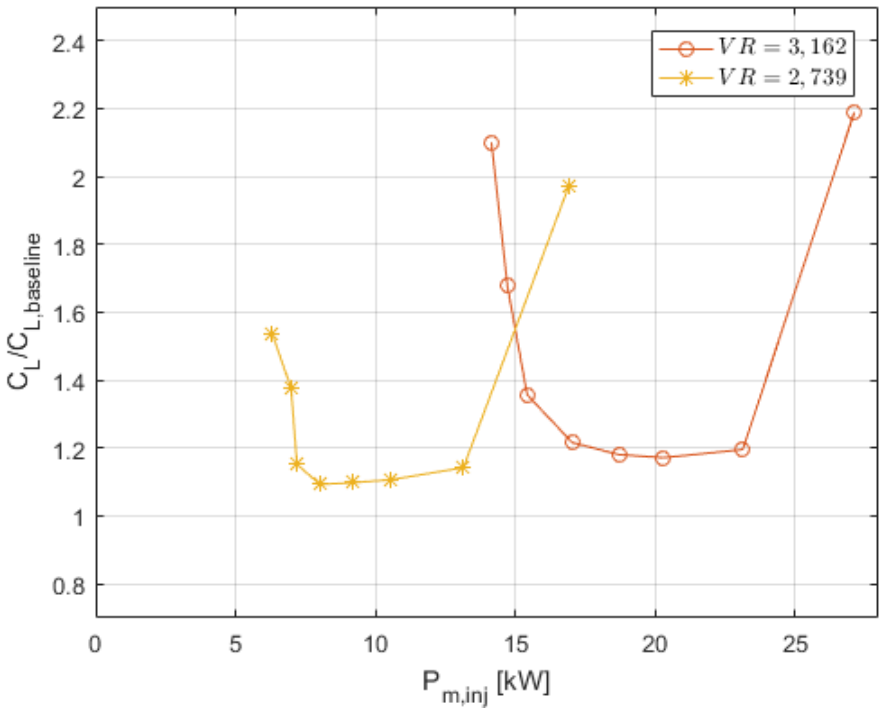

Figure 32: Relative gain of lift compared to the baseline vs required power : $C_\mu = 1{,}5$ %

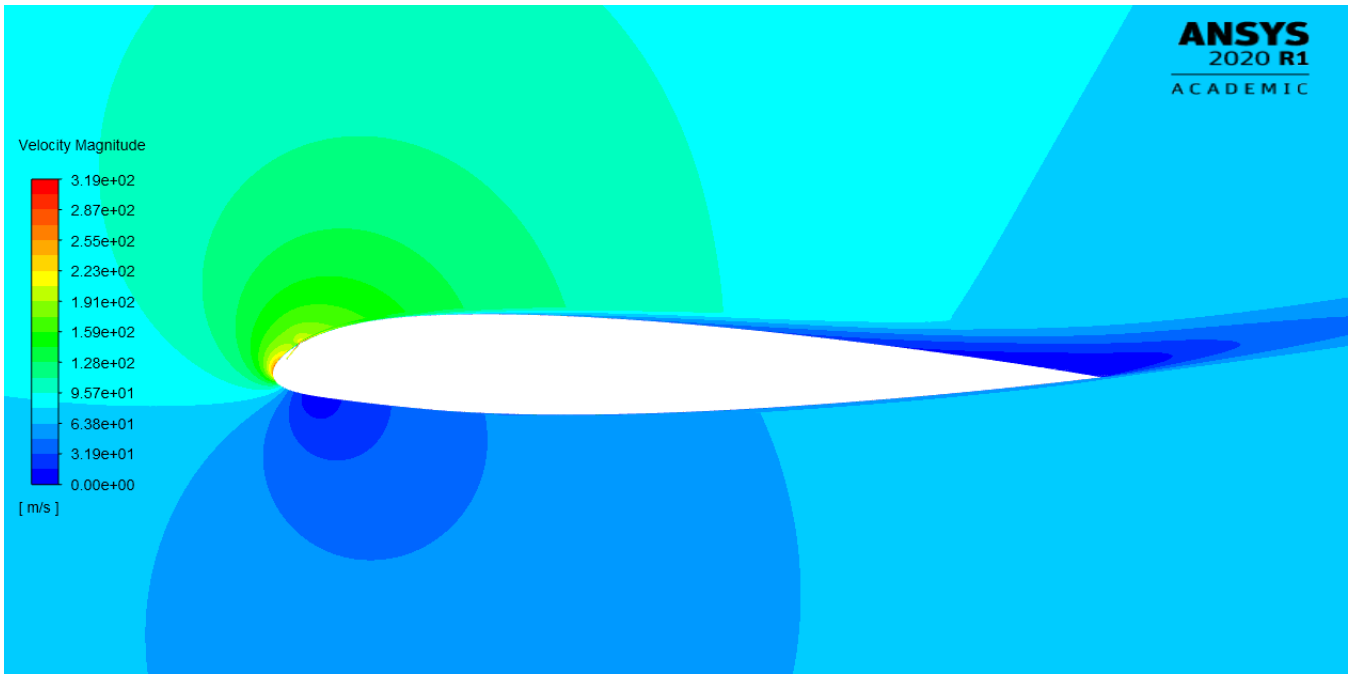

Figure 33: Velocity contour around the airfoil with AFC at $\overline{x}_{inj} = 3$ % : $L_{inj} = 1{,}5$ mm ; $C_\mu = 1{,}0$ % ; VR = 2,582

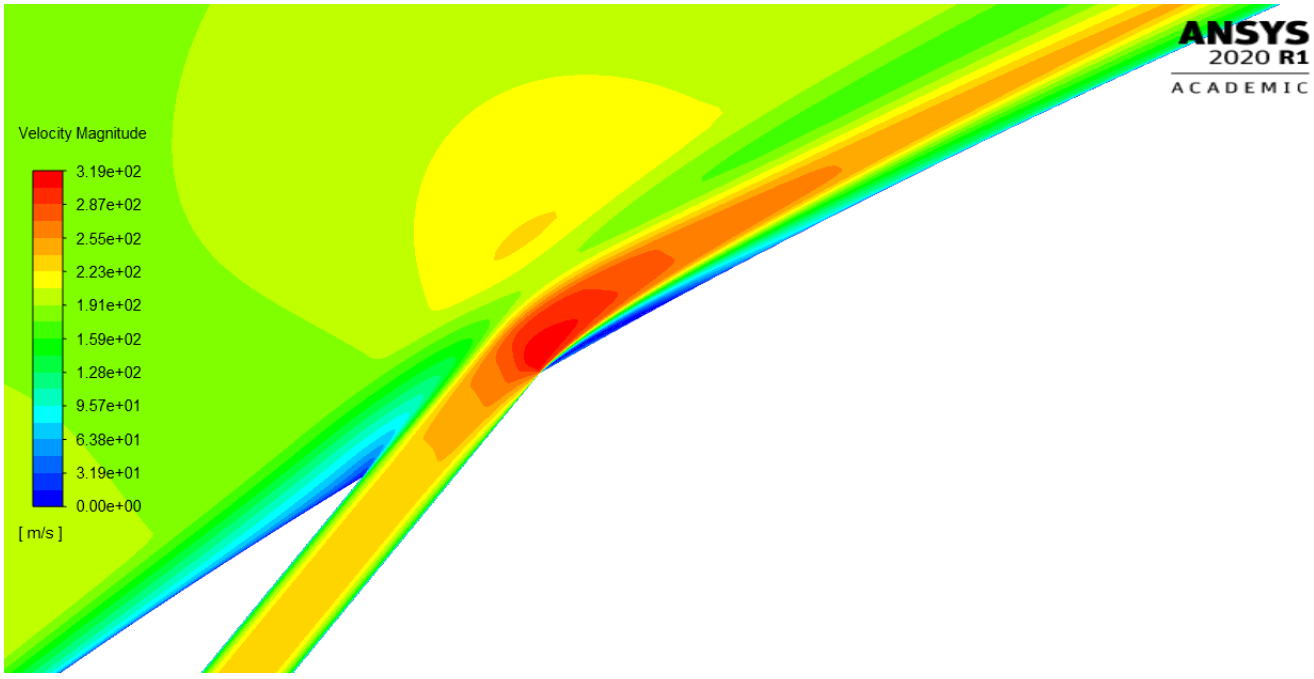

Figure 34: Velocity contour close to the injection slot at $\overline{x}_{inj} = 3$ % : $L_{inj} = 1{,}5$ mm ; $C_\mu = 1{,}0$ % ; VR = 2,582

4.3.2 Impact of the injection slot's position

The next investigated parameter is the position of the blowing channel. Three models with different positions of injection are built : $\overline{x}_{inj} = 2\%$, $\overline{x}_{inj} = 3\%$ and $\overline{x}_{inj} = 4\%$. To try to reinforce the previous conclusions about the momentum coefficient and the velocity ratio, two channel widths are considered : 1,5 mm and 2,0 mm. The velocity ratio is set to get a momentum coefficient of either 1,5 % or 2,0 %. Again, the configurations are computed for the same span of angles of attack as before: 0°, 8°, 12°, 14°, 16°, 18°, 19°and 20°(also 21°sometimes).
The figures 35 to 37 show the comparison between the performances of the airfoil of each configuration. Some observations can be made :

- First, we observe again that for a C_μ of 1,5 %, a thinner injection channel (which means a higher velocity ratio) produces better benefit for the performances of the airfoil, comforting us in the conclusion drawn in the previous part.
- At low angles of attack, the position of injection does not play a part in the lift of the airfoil as we observe again the same flat gain of lift, but with no difference between the $\overline{x}_{inj}$. The differences of the lift between each position of injection does not appear until high angles of attack when the better position is $\overline{x}_{inj} = 4$ % for all configurations.
- The drag of the airfoil at low angles of attack presents some differences as there is more drag when the injection slot is located further from the leading edge. This tendency inverts at higher angles of attack to recover that the best performances (lift and drag coefficients, stalling angle) are at $\overline{x}_{inj} = 4$ % for all configurations.

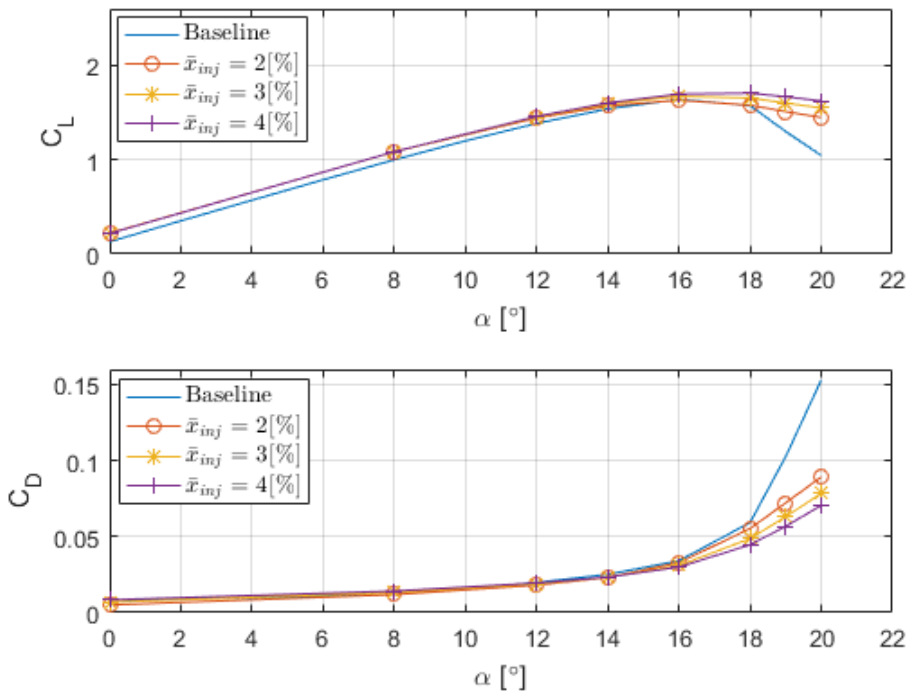

Figure 35: Comparison of the effect of the injection position, lift vs α and drag vs α : $L_{inj} = 1{,}5$ [mm] ; $C_\mu = 1{,}0$ %

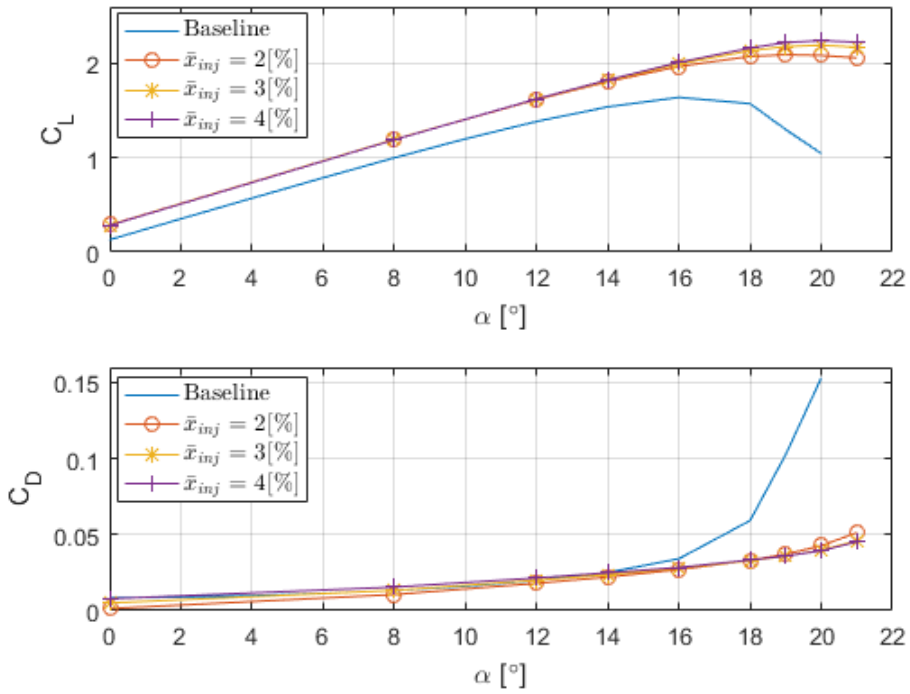

Figure 36: Comparison of the effect of the injection position, lift vs α and drag vs α : L_{inj} = 1,5 [mm] ; C_μ = 1,5 %

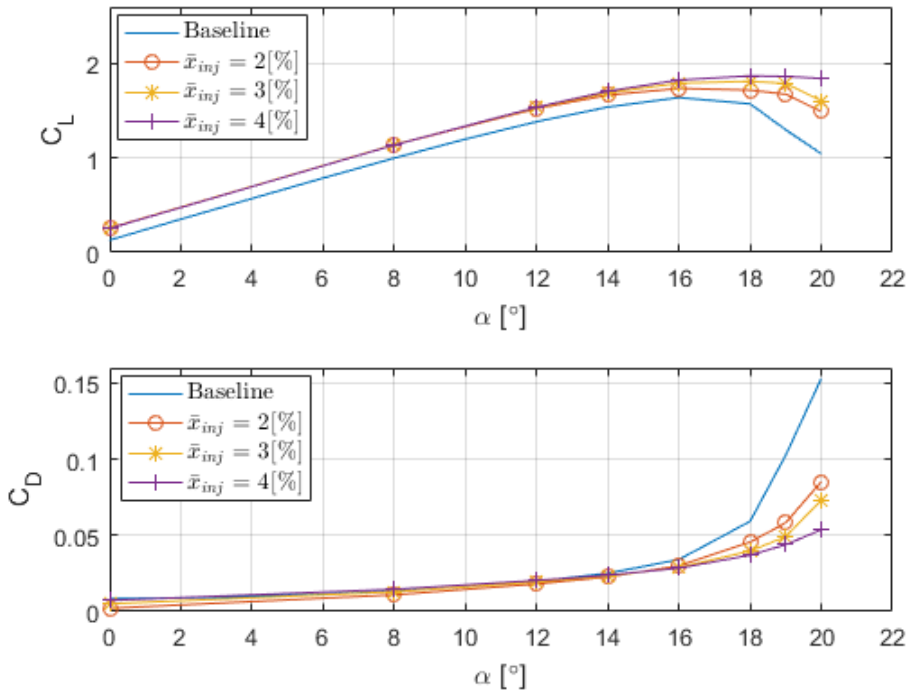

Figure 37: Comparison of the effect of the injection position, lift vs α and drag vs α : L_{inj} = 2,0 [mm] ; C_μ = 1,5 %

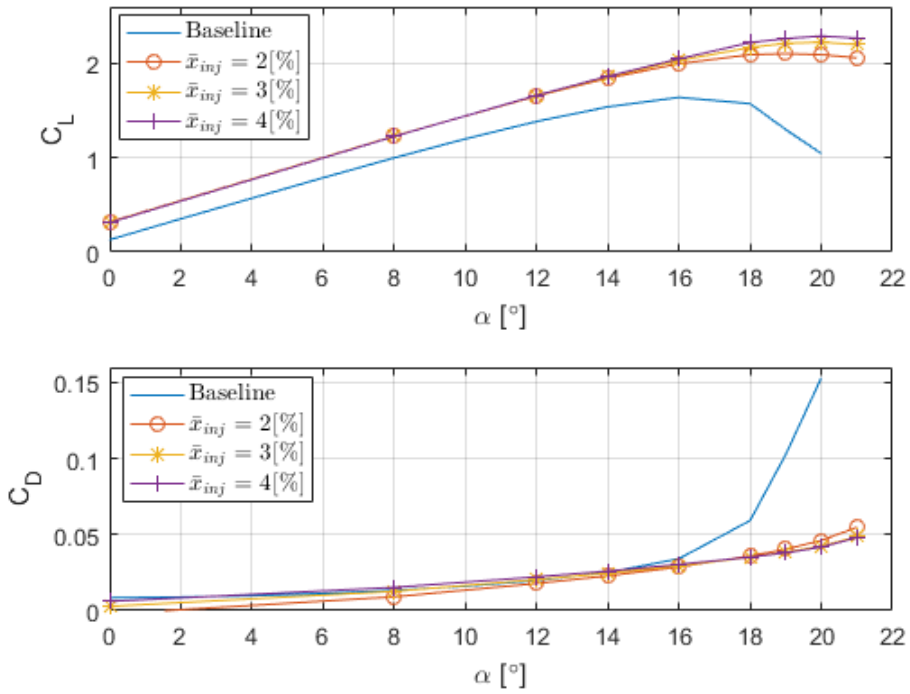

Figure 38: Comparison of the effect of the injection position, lift vs α and drag vs α : L_{inj} = 2,0 [mm] ; C_μ = 2,0 %

4.3.3 Impact of the angle of injection

The last investigated configurations aim at evaluating the impact of the angle of injection relatively to the airfoil's skin. Four angles of injection are considered : 10°, 15°, 20°and 25°. The injection channel for this part has a width of 1,5 mm and two momentum coefficients are used : 1,0% and 1,5%. Multiple configurations with different positions of injection are built to interrogate the conclusions made in the previous part. The figures 39 to 44 show the results of the simulations of all configurations for this part. Here are the observations we can make :

- At low and moderate angles of attack, there is no significant differences between the configurations regarding the produced lift. The angle of injection play no part on the lift produced, but also does the position of injection, as we observed in the previous part. Larger C_μ still adds a greater flat amount of lift.

  There is some differences regarding the drag at low angles of attack : the drag is lower when the angle of injection is higher for all configurations.

- Differences produced by the angle of injection appear at high angles of attack where it appears that there is an optimum of angle of injection (close here to 15°) to provide the higher gain of performances in both lift and drag. The differences are not very large and the angle of injection seems to not play a great part in the effectiveness of the blowing.

- As we observe in the previous part, comparison between the graphs show that the best configuration regarding the position of injection is $\overline{x}_{inj} = 4\%$ as it provide the highest gain of lift at high angles of attack

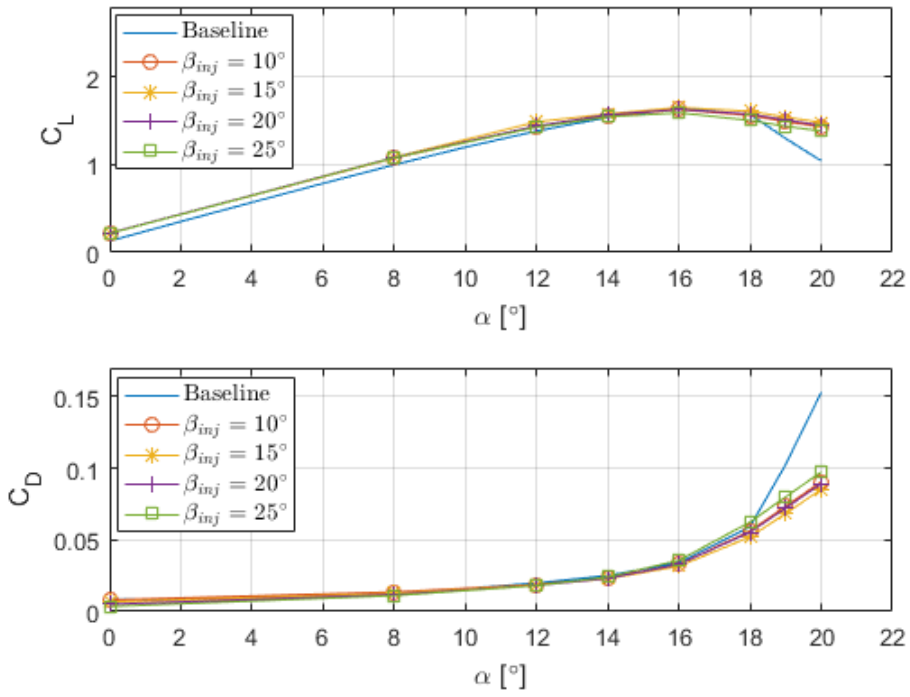

Figure 39: Comparison of the effect of the injection angle : $L_{inj} = 1{,}5$ [mm] ; $C_\mu = 1{,}0$ % ; $\overline{x}_{inj} = 2$ %

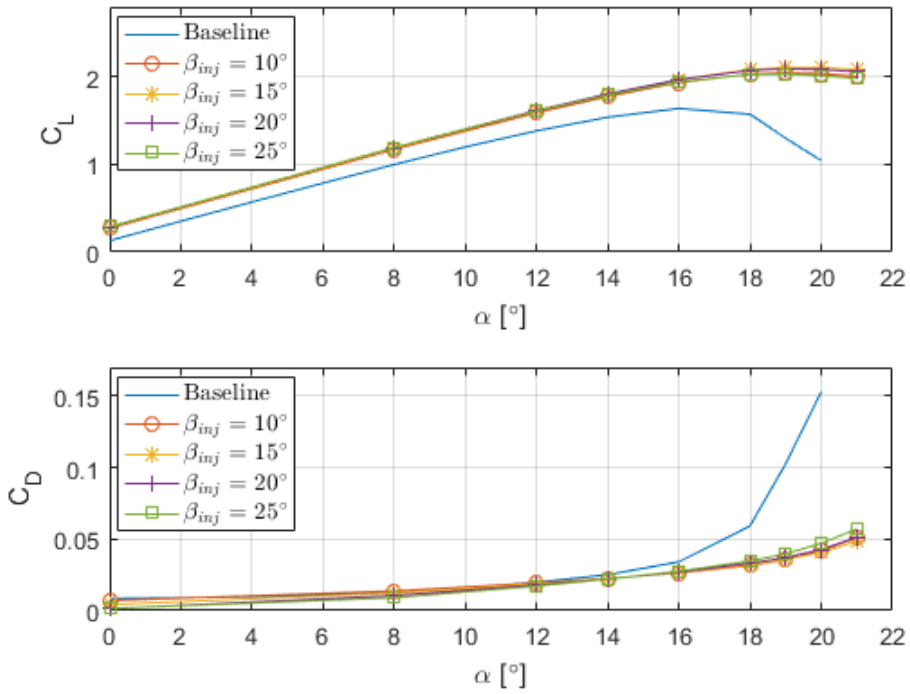

Figure 40: Comparison of the effect of the injection angle : L_{inj} = 1,5 [mm] ; C_μ = 1,5 % ; $\overline{x}_{inj}$ = 2 %

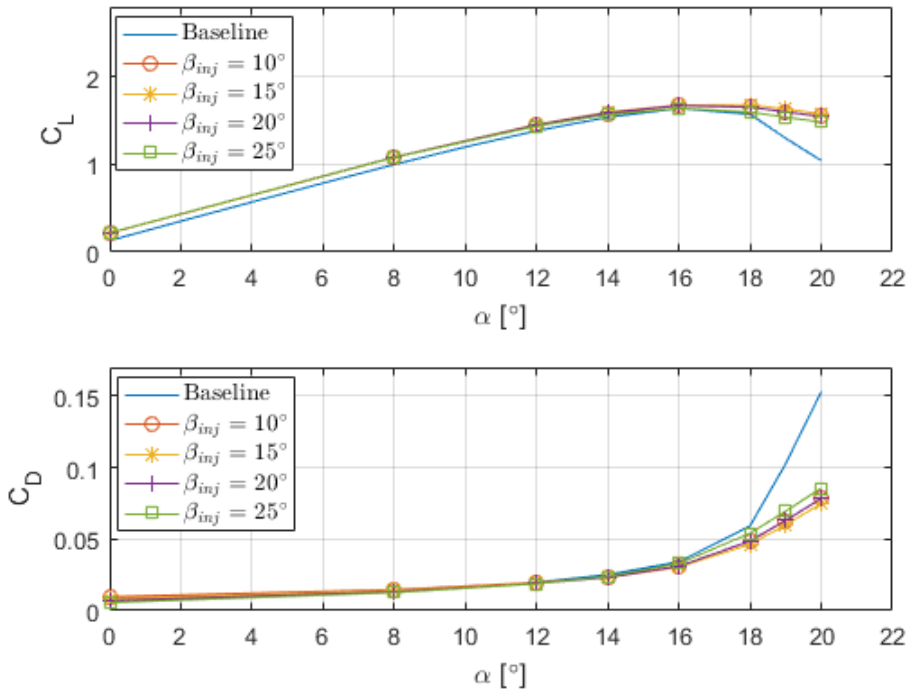

Figure 41: Comparison of the effect of the injection angle : L_{inj} = 1,5 [mm] ; C_μ = 1,0 % ; $\overline{x}_{inj}$ = 3 %

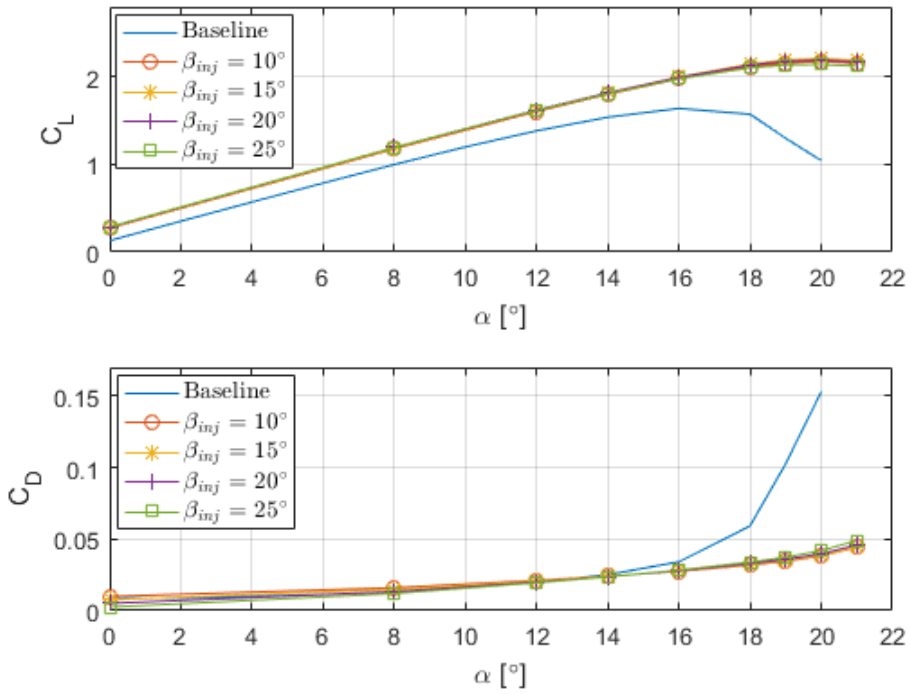

Figure 42: Comparison of the effect of the injection angle : L_{inj} = 1,5 [mm] ; C_μ = 1,5 % ; $\overline{x}_{inj}$ = 3 %

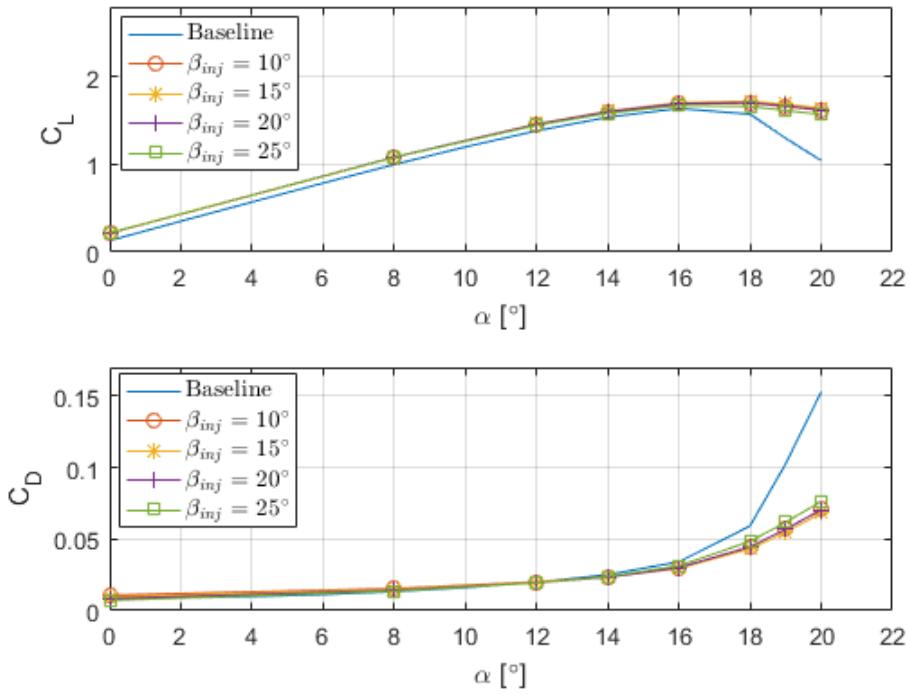

Figure 43: Comparison of the effect of the injection angle : L_{inj} = 1,5 [mm] ; C_μ = 1,0 % ; $\overline{x}_{inj}$ = 4 %

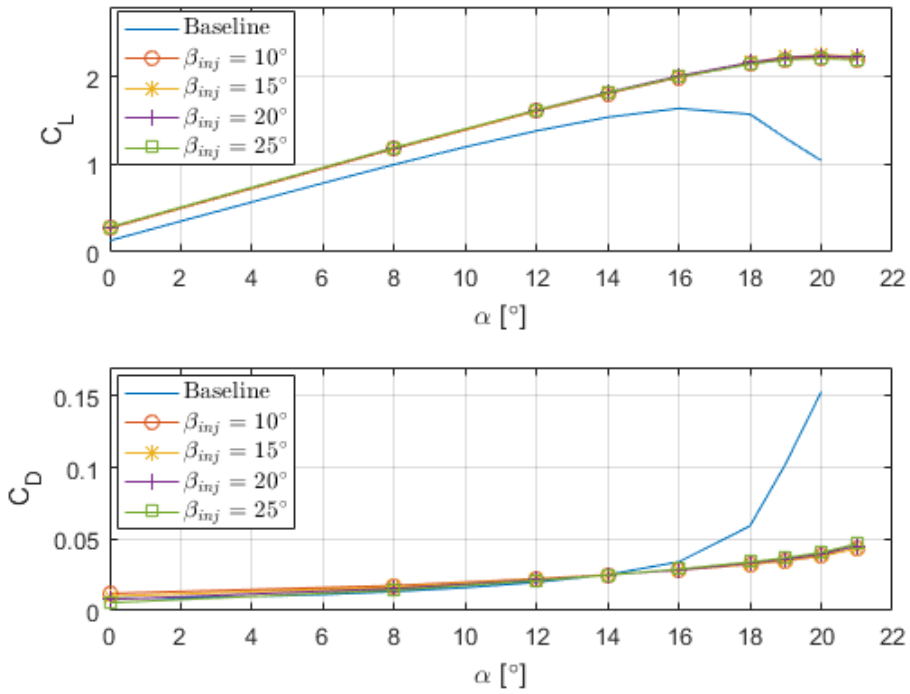

Figure 44: Comparison of the effect of the injection angle : L_{inj} = 1,5 [mm] ; C_μ = 1,5 % ; $\overline{x}_{inj}$ = 4 %

5 Conclusion

The analysis performed in this thesis tried to observe and analyze, using CFD tools, the effects of a specific type of airflow control, the continuous blowing, on the main performances of a NACA23012 airfoil : namely the lift and the drag coefficients. Specific attention was put on the behaviour of the flow separation on the suction side of the airfoil at high angles of attack, main reasons of the reduction of lift at those AoA.

The conditions were set to be similar to an aircraft at low speed like during the take-off and landing. Multiple configurations were built and simulated to analyze the impact of several parameters relative to the blowing : momentum coefficient, velocity ratio, injection channel's width, position of the injection slot and injection angle. Those parameters were separately modified and the best practise were identified in each case, and an estimation of the power required for the blowing to operate was also provided and analyzed.

We conclude that the continuous blowing can greatly improve the performances of an airfoil at high angles of attack, compared to the considered baseline, by delaying the flow separation appearing on the suction side by up to 4°. Higher momentum coefficients provide better benefits, but the velocity ratio plays also a great part in the effectiveness of the control, as too low VR can actually harm the performances of the airfoil. As expected, high benefits were shown to be linked with high power cost.

To extend this work, multiple things can be done :

- To provide more accurate results, a finer mesh can be used. A LES approach of the CFD can also be considered.
- Other configurations of the blowing can be investigated in a comparative study (more complex shape of injection channel, other positions and angles of injection, etc).
- The impact of the roughness of the airfoil's skin can be investigated as well as the inflow Reynolds number.
- Other airfoils can be simulated with continuous blowing to extend the conclusions made here.
- While this analysis focused on one type of fluidic actuator (continuous blowing), other types (sweeping jets, continuous suction, etc) may also be studied and compared to evaluate the best system.

This thesis was also the opportunity for me to improve my understanding and knowledge about airfoils and flow separation. It also introduced me to a new engineering tool of numerical computation : ANSYS fluent that will probably be of use in my professional career.

References

[1] https://donnees.banquemondiale.org/indicator/IS.AIR.PSGR. last consulted on May 2020.

[2] Amhad Batikh ; Lucien Baldas ; Stéphane Colin. "Application of Active Flow Control on Aircrafts - State of the Art". In: *International Workshop on Aircraft System Technologies* (Feb. 2017), p. 7.

[3] https://www.sonaca.com/capabilities/. last consulted on May 2020.

[4] Tuncer Cebec ; G. J. Mosinskis ; A. M. O. Smith. "Calculation of Separation Points in Incompressible Turbulent Flows". In: *Journal of aircraft, Vol. 9, No. 9* (Sept. 1972).

[5] Mehran Tadjfar ; Ehsan Asgari. "Active Flow Control of Dynamic Stall by Means of Continuous Jet Flow at Reynolds Number of 1.10^6". In: *Journal of Fluid Engineering* (Jan. 2018).

[6] David Hue ; Christophe François ; Julien Dandois ; Anna Gebhardt. "Simulations of an aircraft with constant and pulsed blowing flow control at the engine/wing junction". In: *Aerospace Science and Technology, Vol. 69* (2017 October).

[7] A. Gebhardt ; J. Kirz. "Numerical investigation of slot variations on the efficiency of tangential blowing at a vertical tailplane with infinite span". In: *CEAS Aeronautical Journal, Vol. 9* (Feb. 2018).

[8] Timo Kühn ; Vlad Ciobaca ; Ralf Rudnik ; Burkhard Gölling ; Wiebke Breitenstein. "Active Flow Separation Control on a High-Lift Wing-Body Configuration Part 1: Baseline Flow and Constant Blowing". In: *29th AIAA Applied Aerodynamics Conference* (Aug. 2012).

[9] M.G. De Giorgi ; C.G. De Luca ; A. Ficarella ; F. Marra. "Comparison between synthetic jets and continuous jets for active flow control: Application on a NACA 0015 and a compressor stator cascade". In: *Aerospace Science and Technology, Vol. 43* (June 2015).

[10] Chunmei Chen ; Roman Seele ; Israel Wygnanski. "Separation and Circulation Control on an Elliptical Airfoil by Steady Blowing". In: *AIAA Journal, Vol. 50, No. 10* (Oct. 2012).

[11] Bhanu Prakash ; Fernando Mellibovsky ; Josep M Bergada. "Parametric Analysis of Active Flow Control using SteadySuction and Steady Blowing". In: (July 2017).

[12] http://www.airfoiltools.com/airfoil/naca5digit. last consulted on May 2020.

[13] https://www.cfd-online.com/Wiki/Y_plus_wall_distance _estimation. last consulted on May 2020.

[14] Fernando Villalpando ; Marcelo Reggio ; Adrian Ilinca. "Assessment of Turbulence Models for Flow Simulation around a Wind Turbine Airfoil". In: *Advances in Computational Fluid Dynamics and Its Applications* (Apr. 2011).

[15] F. R. Menter ; M. Kuntz ; R. Langtry. "Ten Years of Industrial Experience with the SST Turbulence Model". In: *Heat and Mass Transfer 4* (2003).

[16] Douvi C. Eleni ; Tsavalos I. Athanasios ; Margaris P. Dionissios. "Evaluation of the Turbulence Models for the Simulation of the Flow over a National Advisory Committee for Aeronautics (NACA)0012 Airfoil". In: *Journal of Mechanical Engineering Research Vol. 4* (Mar. 2012), pp. 100–101.

[17] M. Bauer. "Design and Application of a Fluidic Actuator System for high-lift Flow Control". In: (2015).

[18] M. Jabbal S. C. ; Liddle ; W. J. Crowther. "Active Flow Control Systems Architectures for Civil Transport Aircraft". In: *Journal of Aircraft, Vol. 47, No. 6* (Nov. 2010).

[19] Ira H. Abbott ; Albert E. Von Doenhoff. "Theory of Wing Sections, Including a Summary of Airfoil Data". In: (1959), pp. 143, 148, 498–499.

[20] A.A. Abdhel Rahman ; W.M. Chakron. “Surface Roughness Effects on Flow over Airfoil”. In: *Wind Engineering; Vol. 21, No. 3* (1997).

[21] F. Rasi ; M.R. Soltani. “Effect of Leading-Edge Roughness on Boundary Layer Transition of an Oscillating Airfoil”. In: *Scientia Iranica, Vol. 20, No. 3* (June 2013), pp. 508–515.

UNIVERSITÉ CATHOLIQUE DE LOUVAIN
École polytechnique de Louvain
Rue Archimède, 1 bte L6.11.01, 1348 Louvain-la-Neuve, Belgique | **www.uclouvain.be/epl**